



Two decades of pH_T measurements along the GO-SHIP A25 section 1

- Fiz F. Pérez¹, Marta López-Mozos^{1,2*}, Marcos Fontela¹, Maribel I. García-Ibáñez³, Noelia Fajar⁴, Xosé 2
- Antonio Padín¹, Mónica Castaño-Carrera¹, Mercedes de la Paz¹, Lidia I. Carracedo⁵, Marta Álvarez⁶, 3
- Pascale Lherminier⁵, Antón Velo^{1*} 4
- 5 6 7 8 9 ¹Instituto de Investigaciones Marinas (IIM), CSIC, Vigo, 36208, Spain
- ²Facultad de Ciencias del Mar, Universidade de Vigo, Spain
- ³Centro Oceanográfico de Illes Balears (COB-IEO), CSIC, Palma, Spain
- ⁴Centro Oceanográfico de Vigo (COV-IEO), CSIC, Vigo, Spain
- ⁵University of Brest, CNRS, Ifremer, IRD, Laboratoire d'Océanographie Physique et Spatiale (LOPS), IUEM, Plouzané,
- 10 29280, France
- 11 ⁶Centro Oceanográfico de A Coruña (COAC-IEO), CSIC, A Coruña, Spain
- 12 *Correspondence to: Marta López-Mozos (mlopezm@iim.csic.es) and Antón Velo (avelo@iim.csic.es)

13 **Abstract**

- 14 The North Atlantic (NA) GO-SHIP A25 OVIDE-BOCATS section is a long-term repeat hydrographic transect
- 15 extending from Portugal to Greenland. Since 2002, physical and biogeochemical measurements have been carried
- out biennially along the OVIDE-BOCATS section, contributing to a better understanding of water mass properties, 16
- 17 mixing, circulation, carbon storage, and climate change impacts such as ocean acidification (OA) in the NA. In
- particular, the high-precision pH measurements on the total hydrogen ion scale (pH_T) from the OVIDE-BOCATS 18
- 19 program represent a key milestone in monitoring OA in this particularly climate sensitive region. The method used
- 20 for pH_T determination relies on adding meta-cresol purple (mCP) dye to the seawater sample and
- 21 spectrophotometrically measuring its absorbances at specific wavelengths. The OVIDE-BOCATS program has
- 22 used unpurified mCP dye, which impurities have been proven to bias pH_T values. Here we quantified the bias
- 23 induced by these impurities in pH_T measurements. We found that measurements carried out using the unpurified
- 24 mCP dye tend to be, on average, 0.011 ± 0.002 pH_T units higher than those obtained using the purified mCP dye,
- 25 with this difference slightly decreasing at higher pH_T values. Moreover, we tested independent methods to correct
- 26 the effect of impurities in both the historical and recent OVIDE-BOCATS pH_T data, demonstrating that the 27
- correction is consistent across methods. The long-term pH_T dataset has been updated to include newly acquired 28 data and absorbance measurements, and to standardize corrections for mCP dye impurities. This effort results in a
- 29 twenty-year dataset of pH_T corrected for mCP dye impurities, that demonstrates the possibility of a global effort to
- 30 improve the reliability and coherency of spectrophotometric pH_T measurements made with unpurified mCP dye.
- 31 The corrections applied to our pH_T dataset have negligible implications for the OA rates previously reported, but
- 32 they do affect the depth of the aragonite saturation horizon, implying a shoaling of approximately 150 m.

1 Introduction

- 35 The oceanic absorption of anthropogenic CO₂ (C_{ant}) is causing major changes in the marine carbonate system chemistry (Friedlingstein et al., 2023; Le Quéré et al., 2015). The ocean is slightly basic generally; however, Cant 36
- 37 uptake increases the concentration of total hydrogen ions ($[H^+]_T$), decreasing pH and the concentration of carbonate
- 38 ions. These changes are collectively referred to as ocean acidification (OA) (Caldeira and Wickett, 2003; Orr et al.,
- 39 2005), and they are especially detrimental for calcifying marine organisms and their ecosystems (IPCC, 2019). OA
- 40 is a major concern for decision-makers at both local and global scales due to its potential impacts on marine





ecosystem health and food security (Gattuso et al., 2015). The future impact of OA will depend on variations in the long-term mean and the short-term temporal variability of the marine carbonate system (Kwiatkowski & Orr, 2018).

Due to their physicochemical characteristics, surface waters in polar and subpolar regions are expected to experience the greatest OA impact (IPCC, 2019; Orr et al., 2005). However, the impact of OA is not limited to surface waters. Recent observations have shown that intermediate layers of the North Atlantic (NA) are experiencing higher OA rates than surface waters (Pérez et al., 2021; Resplandy et al., 2013) due to its distinctive circulation dynamics. The upper limb of the Atlantic Meridional Overturning Circulation (AMOC) transports C_{ant} from the subtropics to the Subpolar North Atlantic (SPNA), where it is transferred to intermediate and deep layers—with lower buffering capacity than surface layers—through deep winter convection and water mass formation (Asselot et al., 2024). This process would ultimately contribute to the deterioration of NA deep-water coral ecosystems (Fontela et al., 2020a; García-Ibáñez et al., 2021; Gehlen et al., 2014; Perez et al., 2018).

The demand for open-access OA data is increasing, driven by United Nations Sustainable Development Goal (SDG) 14 and by its role as a climate indicator recognized by the World Meteorological Organization (WMO). Although great progress in autonomous marine data collection has been achieved in recent years (Bushinsky et al., 2025), high-quality, ship-based pH measurements remain essential for ensuring the reliability of OA data collected by sensors on autonomous platforms, such as Argo floats and moorings, by enabling rigorous calibration protocols that correct for potential biases over time due to sensor drift, biofouling, and pressure effects (Ishii et al., 2025; Maurer et al., 2021; Pérez et al., 2023; Takeshita et al., 2018).

Despite the critical role of pH data in understanding OA, significant limitations exist within key ocean databases such as the Global Ocean Data Analysis Project (GLODAPv2) (Olsen et al., 2016; Key et al., 2015). In GLODAPv2, pH data that is reported on the total hydrogen ion scale (pH_T)—which accounts for both the aqueous hydrogen ions (H₃O⁺) and the associated form with sulfate ions (HSO₄⁻)—and have historically been collected less frequently than other carbonate system variables, such as total alkalinity (A_T) and total dissolved inorganic carbon (C_T) (Key et al., 2015; Lauvset et al., 2024; Olsen et al., 2019). A_T and C_T measurements are generally considered more reliable due to the availability of standardized reference materials, consensually accepted methods, and quality control procedures. In contrast, although pH_T measurements are technically precise, easy to perform, and cost-effective, their intercomparability is more challenging, arising from methodological inconsistencies across various research initiatives (Dickson et al., 2015; Ma et al., 2019; Álvarez et al., 2020; Capitaine et al., 2023). These factors contribute to the relative scarcity of pH_T measurements in GLODAPv2, and lead to the future GLODAPv3 providing pH_T data as originally reported with no additional internal consistency corrections, a limitation that may potentially affect the reliability of OA analysis from directly measured pH_T data instead of those calculated from A_T and C_T (Álvarez et al., 2020; Carter et al., 2024b).

Briefly, the spectrophotometric pH method is a straightforward technique that involves adding an acid-base indicator dye, usually meta-cresol purple (mCP), to the seawater sample. The method was defined in the 1990s (Clayton & Byrne, 1993) and has been updated since then, and still lacks metrological traceability and reference materials (Ma et al., 2019; Carter et al., 2024a). The method is based on the distinct absorbance wavelengths of the indicator dye's acid and basic forms, which are used to calculate an absorbance ratio. Subsequently, pH_T is calculated using the indicator dye's dissociation constant and its extinction coefficients through a parameterization in function of temperature and salinity, relating the absorbance ratio with pH_T . This method offers a high degree of precision (error even lower than ± 0.001 pH units), with an approximate total uncertainty of ± 0.01 pH_T units (Dickson, 2010; Carter et al., 2024a). A primary source of error in these pH_T measurements arises from the impurities present in the mCP dye itself (Liu et al., 2011). Over the last decade, different studies proved that mCP



88

89

90

91

92

93

94

95 96

97

98

99

100

101

102

103

104

105

106

107

108

109

110

111 112

113



impurities cause the measured pH_T to exhibit a bias that is dependent on the sample's pH_T and the brand and batch of the mCP dye used (Liu et al., 2011; Yao et al., 2007). Consequently, mCP was proposed to be purified (Liu et al., 2011; Rivaro et al., 2021) to remove these impurities and parameterizations re-evaluated for those purified mCP dyes (Liu et al., 2011; Loucaides et al., 2017; Müller et al., 2018). Although some laboratories, mostly in the US, currently use purified mCP dye (Carter et al., 2018), purified mCP dyes are not commercially available, being scarce and expensive, and therefore not affordable for all laboratories. Alternatively, it is possible to evaluate the effect of these impurities on the absorbance values and correct them accordingly (Douglas & Byrne, 2017; hereafter DB'17; Takeshita et al., 2020, 2021; Woosley, 2021).

Over the past two decades, the GO-SHIP A25 OVIDE-BOCATS ship-based hydrographic section (OVIDE-BOCATS hereafter; see Sect. 2.1)—the only transoceanic cruise with a biennial frequency in the CLIVAR and GO-SHIP programs—has built an extensive pH_T time series in the NA of more than 23,500 pH_T samples measured using unpurified mCP dye. During the 11 OVIDE-BOCATS cruises, pH_T was measured spectrophotometrically following a consistent methodology and using the same commercial mCP dye brand, Sigma-Aldrich, which—like other commercial brands—contains impurities (Liu et al., 2011; Yao et al., 2007). As awareness of pH_T biases introduced by mCP impurities has grown, so has the need to assess and correct their impact to ensure the internal consistency and long-term comparability of the OVIDE-BOCATS pH_T dataset. In this context, we evaluated the bias induced by these impurities by carrying out measurements with purified and unpurified mCP dyes, and assessed independent methods to account for and correct the effect of these impurities in both the historical and contemporary OVIDE-BOCATS pH_T data. Here we present (1) the new data from the last two BOCATS cruises of 2021 and 2023, (2) the absorbance measurements along with the evaluation of the impurities effect on them, and (3) the entire OVIDE-BOCATS pH_T database product since 2002, consistently adjusted for impurity-related bias. This effort allowed us to evaluate—in a consistent way—the OA rates in the NA and to improve the reliability of

the pH_T data collected to date, which is fundamental for understanding the ocean's response to climate change.

2. Methods

2.1 OVIDE-BOCATS transoceanic section

- 114 The OVIDE-BOCATS section is a high-quality hydrographic transect in the NA, extending from Portugal to
- 115 Greenland and largely following the GO-SHIP A25 track (Fig. 1), with the objective of studying the SPNA region.
- 116 Initially focused on physical oceanography (Mercier et al., 2024), its scope rapidly expanded to include critical 117
- aspects of the carbon cycle, such as OA and the uptake and storage of Cant in the SPNA—one of the ocean's largest
- 118 C_{ant} reservoirs (Sabine et al., 2004). Since 2002, in situ physical and on-board biogeochemical measurements have
- 119 been performed biennially along the OVIDE-BOCATS section. This repeated section is one of the longest-standing 120 and most frequently revisited transects within the GO-SHIP and CLIVAR programs. Accordingly, data
- 121 follows policies, publicly management strict and all datasets are available
- 122 (https://www.ncei.noaa.gov/access/ocean-carbon-acidification-data-
- 123 system/oceans/RepeatSections/clivar ovide.html).

124 125 Thanks to its high frequency of repeated occupations, the OVIDE-BOCATS dataset offers a unique opportunity to

- 126 study the biennial evolution of NA processes. The program focuses on water mass properties, mixing, and
- 127 circulation; the impact of climate events on NA dynamics; volume and heat transports; and AMOC variability. 128 Particular attention is given to investigate key water masses such as Subpolar Mode Water (SPMW) and Labrador
- 129 Sea Water (LSW)—both formed through deep winter mixing in the SPNA— as well as Denmark Strait Overflow



Water (DSOW) and Iceland-Scotland Overflow Water (ISOW)—both resulting from the entrainment of SPMW and LSW into the overflows at the sills between Greenland, Iceland, and Scotland, respectively (García-Ibáñez et al., 2015; Lherminier et al., 2010).

Research within the OVIDE-BOCATS framework has also focused on carbon inventories and the deep biogeochemical imprint, such as the role of the Deep Western Boundary Current (DWBC) in transporting oxygen, nutrients, and dissolved organic carbon (Álvarez-Salgado et al., 2013; Fontela et al., 2019; 2020b). In addition, OVIDE-BOCATS has evaluated OA rates in the NA (Fontela et al., 2020a; García-Ibáñez et al., 2016; Vázquez-Rodríguez et al., 2012) and analyzed its impact on marine biodiversity (Pérez et al., 2018; García-Ibáñez et al., 2021) as well as the ocean's capacity to absorb, store, and transport CO₂ (Pérez et al., 2013; Zunino et al., 2015). In summary, the sustained observations from the OVIDE-BOCATS program demonstrated to be essential for detecting OA trends, improving climate models, and understanding the SPNA's response to climate change (Rodgers et al., 2023).

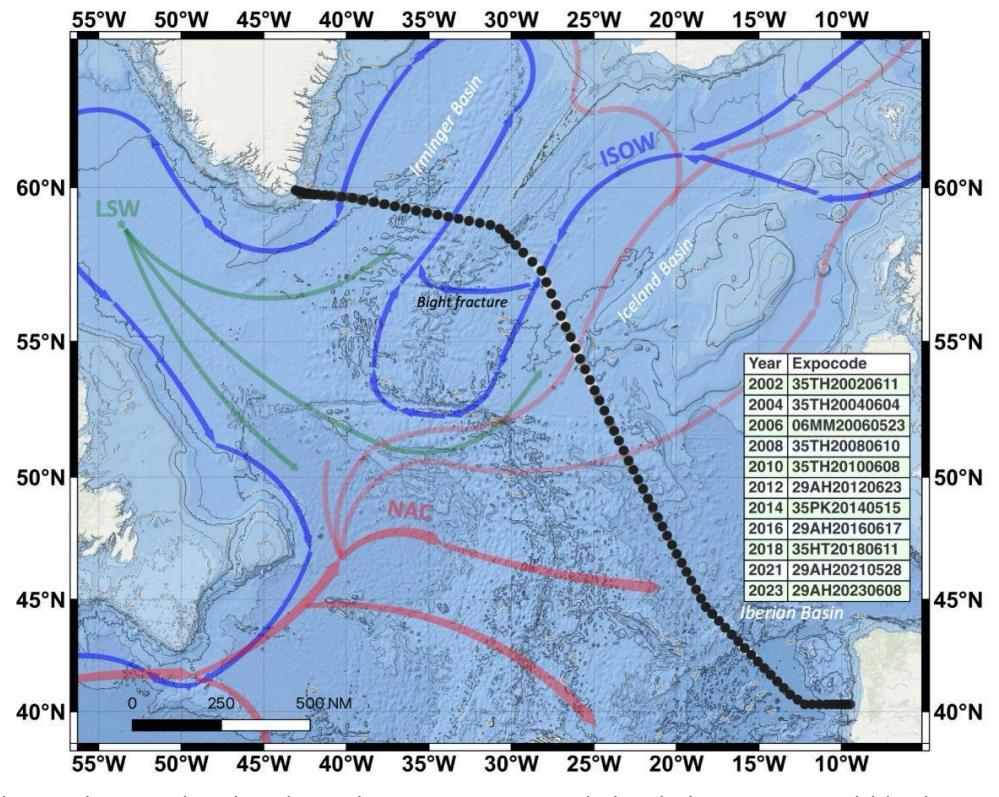


Figure 1. Bathymetric map showing the main water masses and circulation patterns within the SPNA region covered by the OVIDE-BOCATS section (station locations indicated by black dots). The inset table lists each biannual cruise along with its corresponding expocode as identified in GLODAP. Major currents and water masses are illustrated in different colors according to their temperature and depth (from red—warmer and shallower—to blue—colder and deeper). The main schematized currents and water masses include the North Atlantic Current (NAC), Labrador Sea Water (LSW), and Iceland-Scotland Overflow Water (ISOW). The principal basins traversed along the OVIDE-BOCATS section, from west to east, are the *Irminger*, *Iceland*, and *Iberian basins*.





152 2.2 pH_T determination

2.2.1 Spectrophotometric pH_T method fundamentals

In all OVIDE-BOCATS cruises, pH_T was measured manually following the spectrophotometric method proposed by Clayton and Byrne (1993)—hereafter CB'93. This method involves adding a mCP dye solution to the seawater sample and calculating the sample's pH_T using the following equation:

$$pH_{T} = pK_{2} + \log_{10} ([I^{-2}] / [HI^{-}])$$
 (1),

where [HI⁻] and [I₂⁻] represent the concentrations of mono-dissociated and bi-dissociated species of the indicator dye, respectively. The concentration ratio ([I⁻²] / [HI⁻]) can be determined spectrophotometrically by measuring absorbance at the corresponding maximum absorbance wavelengths (A), i.e., 434 nm and 578 nm, respectively, corrected for baseline absorbance at 730 nm—hereafter referred to as $_{434}$ A, $_{578}$ A, and $_{730}$ A, respectively. pH_T is then calculated using CB'13 parameterization of Eq. (1):

$$pH_{T} = 1245.69/T + 3.8275 + (2.11 \cdot 10^{-3}) \cdot (35 - S) + \log ((R - 0.0069) / (2.222 - 0.133 \cdot R))$$
 (2),

where *T* is temperature in Kelvin, *S* is salinity, and *R* is the ratio of the absorbances of the mono-dissociated and bi-dissociated forms of the indicator dye corrected for baseline absorbance:

$$R = ({}_{578}A - {}_{730}A) / ({}_{434}A - {}_{730}A)$$
(3).

The first three terms of Eq. (2) represent the second dissociation constant of mCP dye (pK₂). The pK₂ obtained by CB'93 is based on the *TRIS* buffer characterization of Dickson (1993), which used electromotive force data from Ramette et al. (1977). DelValls and Dickson (1998)—hereafter DVD'98—later determined that the pH_T values assigned to *TRIS* buffers needed to be increased by 0.0047, for all temperatures and salinities. These corrected *TRIS* pH_T values have recently been confirmed by Müller et al. (2018). Consequently, spectrophotometric pH_T values obtained using the CB'93 parameterization should be adjusted by +0.0047 pH_T units (Lee et al., 2000).

The CB'93 parameterization was developed using Kodak mCP dye, which contained impurities presenting significant absorbance at 434 nm (referred to as 434 A_{imp}). However, it was not until the 2000s that the impact of impurities on pH_T measurements was evidenced. Specifically, Yao et al. (2007) compared pH_T determinations using Sigma-Aldrich and Kodak mCP dyes with TRIS buffers, finding that pH_T values obtained with Sigma-Aldrich mCP dye were between 0.001 to 0.006 pH_T units higher than those with Kodak mCP dye (for pH_T ranging from 7.4 to 8.2), attributed to lower 434Aimp values in the Sigma-Aldrich mCP dye. Later, Liu et al. (2011; hereafter L'11) purified mCP dye and developed a new parameterization to determine pH_T from R, demonstrating that applying their new parameterization to R data measured with impure mCP dye results in pH_T values up to 0.015 pH_T units lower. Subsequently, Loucaides et al. (2017) and Müller et al. (2018) produced very similar parameterizations, extending the valid salinity and temperature ranges and confirming the same pH_T versus R relationship at 25°C and oceanic salinities (see Fig. S1 in Alvarez et al., submitted). Thus, ideally, pH_T measurements should be performed using purified, well-characterized mCP dyes and following a consensus method that ensures traceability to the International System of Units (SI; Capitaine et al., 2023). However, the purification procedure is not accessible to many laboratories routinely measuring seawater pH_T. To overcome this limitation and facilitate high-quality spectrophotometric pH_T measurements, DB'17 proposed a method to determine 434A_{imp} and an associated correction procedure. This approach allows to compute the R corrected for the impurities contribution at 434A (i.e., 434A_{imp}),

 $\begin{array}{c} 210 \\ 211 \end{array}$

and consequently enables pH_T calculations using parameterizations derived for purified mCP dye, such as the L'11 parameterization.

What is the bias introduced in pH_T measurements as a result of mCP dye impurities? Most of the spectrophotometric pH_T values in GLODAPv2 (Lauvset et al., 2024) are calculated using the CB'93 parameterization, based on measurements made with mCP dyes that contain impurities. Figure 2 shows a family of curves representing the theoretical differences between pH_T values calculated using the CB'93 parameterization with R values that would have been obtained with unpurified mCP dyes (i.e., with varying $_{434}A_{imp}$), and those obtained using the L'11 parameterization applied to R values corresponding to a fully purified mCP dye (i.e., $_{434}A_{imp} = 0$). We computed the corresponding $_{434}A$ values ($_{434}A_{pur}$, i.e., $_{434}A_{imp} = 0$) using the relationship described in Sect. 2.2.4 for a set of theoretical purified R ($_{pur}$) values ranging from 0.3 to 2.6. Both the purified R values and their associated $_{434}A$ values were then used in Eq. (11) of DB'17 to compute the adjusted R values ($_{unpur}$) that reflect the contribution of mCP dye impurities ($_{434}A_{imp} \neq 0$) as follows:



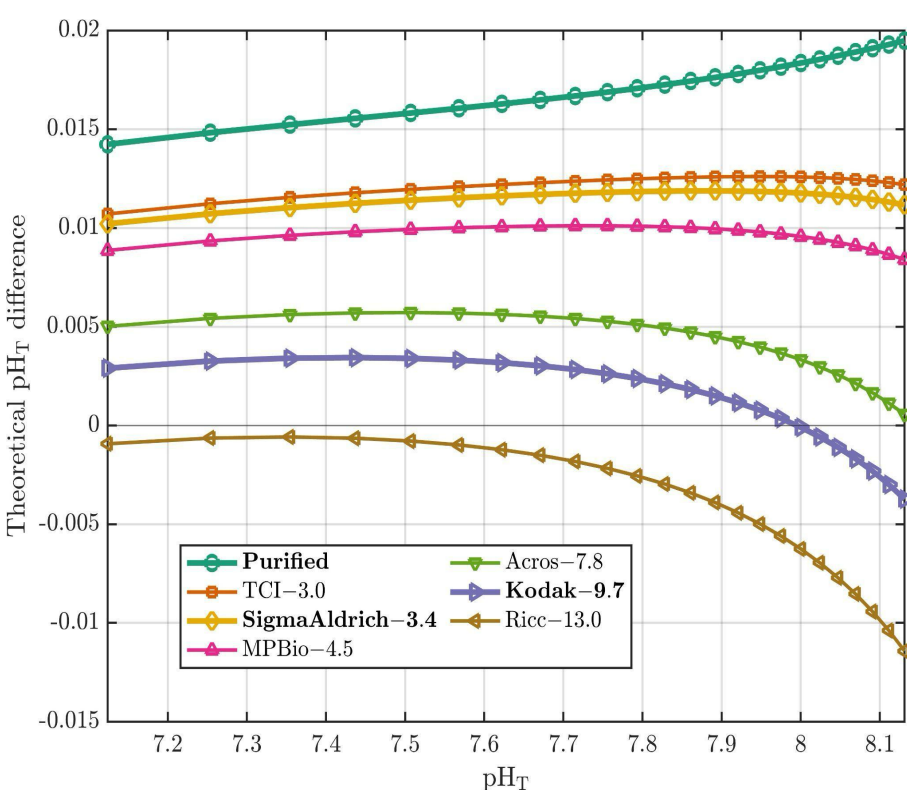


Figure 2. Theoretical differences in pH_T (y-axis) between values using the CB'93 parametrization with the DVD'98 correction (applied to R values derived from mCP dyes with varying impurities) and those calculated using the L'11 parametrization (applied to R values derived from a purified mCP dye). The differences are plotted against pH_T computed using the L'11 parameterization (x-axis), at S = 35 and T = 25°C. Each mCP dye is represented by a different color, with its corresponding $_{434}A_{imp}$ value (in units of 10^{-3} absorbance) listed after the indicator dye name. Bold indicates mCP dye brands discussed in this work. All $_{434}A_{imp}$ values are taken from DB'17, except for Sigma-Aldrich, whose value was determined in this study.





The mCP dye brands and their corresponding absorbance values due to their impurities, as shown in Fig. 2, are primarily taken from Table 2 of DB'17, that are based on an mCP dye concentration of 3.3 µM in the sample cell. When the CB'93 parameterization is applied to R_{unpur} at S = 35 and 25°C, the largest theoretical pH_T differences (> 0.015 pH_T units) are observed relative to pH_T values obtained by applying the L'11 parametrization to the corresponding R_{pur} under the same conditions (see turquoise line in Fig. 2). In contrast, when CB'93 parametrization is applied to R_{unpur} values obtained with Kodak mCP dye, the resulting pH_T values differ by only ±0.003 pH_T units from those obtained with the L'11 parameterization with a purified mCP dye, with minimal differences observed in the pH_T range of 7.65 to 8.15 (purple line in Fig. 2). This agreement arises because the CB'93 parametrization— developed using Kodak mCP dye and calibrated against TRIS buffers using unpurified mCP dye—yields lower R values than that obtained with purified mCP dye. As a result, both parameterizations converge around the TRIS buffer pH_T value (8.093 at 25°C; DVD'98). Indeed, Fig. 2 shows that larger biases in the final pH_T arise when using the CB'93 parameterization with mCP dyes with lower impurity content, while the magnitude and pH_T-dependence of these biases increases with higher impurity levels.

2.2.2 pH_T sampling and manual spectrophotometric procedure during the OVIDE-BOCATS cruises

On all OVIDE-BOCATS cruises, seawater samples for pH_T were collected after oxygen samples, using 100 mm pathlength cylindrical optical glass cells with two stoppers (Dickson et al., 2007). Each sample was taken by rinsing the optical cell twice and flushing it with seawater two or three times its volume, ensuring no air bubbles remained. To achieve this, the cell was held with the outlet above the inlet, the outlet was plugged first, the sampling tube was removed, and the second plug was inserted—taking care to avoid air bubbles. After rinsing and externally drying the cells, they were placed in a thermostatic incubator set at 25°C for at least 30—45 minutes to ensure temperature stabilization at 25°C prior to their measurement.

For each sample, a blank measurement was performed after drying and cleaning both faces of the optical cell and placing it in the spectrophotometer's cell holder. Following blanking with sampled seawater, 75 μ L of 2 mM mCP dye solution were added to each 28 mL sample cell using an adjustable repeater pipette (SOCOREX), resulting in a final mCP dye concentration of 5.36 μ M in the cell. Dispenser syringes were wrapped in aluminum foil to prevent photodegradation of the mCP dye (Fontela et al., 2023). After the mCP dye addition, the cell was thoroughly shaken and placed back in the holder maintaining the same orientation as for the blanking. Triplicate absorbance measurements were carried out at the three target wavelengths (434 nm, 578 nm, and 730 nm). All absorbance readings were carried out in the spectrophotometer's thermostatted cell compartment, maintained at 25.0 \pm 0.2°C.

Byrne & Breland (1989) demonstrated that pH_T determinations are largely insensitive to temperature variations; specifically, R values between 0.7 and 2 exhibit a pH_T error of less than 0.001 pH_T units per 1°C change when using the CB'93 parameterization. This insensitivity arises because the temperature dependence of pK_2 of the mCP dye closely matches the temperature effect on pH_T . Nevertheless, it is recommended to ensure that temperature deviations remain within ± 0.5 °C of the reference temperature (25°C). In our procedure, sample temperature was monitored every five measurements to confirm that it remained within this tolerance range.

2.2.3 Effect of the indicator dye addition and spectrophotometer performance on the pH_T measurements

Throughout the OVIDE-BOCATS program, the mCP dye used was from Sigma-Aldrich (Cat. No. 11,436-7 in the basic form; C₂₁H₁₇NaO₅S; molecular weight 404.41 g). Prior to 2018, mCP dye solutions were prepared by dissolving 0.080 g of the mCP sodium salt in 100 mL of natural seawater. Following DB'17 recommendations, the preparation method was modified in 2018, with the mCP dye being dissolved in 0.7 M NaCl instead of seawater.





The absorbances of the mCP dye solutions at 434 nm, 578 nm, and 730 nm were measured spectrophotometrically using a 0.1 mm optical cell to ensure that the R values remained close to 1, corresponding to a pH_T of approximately 7.67 (Li et al., 2020). mCP dye solutions were stored in Pyrex bottles, refrigerated, and protected from light using aluminum foil.

The addition of the indicator dye slightly perturbs the sample's pH_T, with the magnitude of this effect increasing for shorter optical pathlengths and when the pH_T difference between the sample and the indicator dye is large (Chierici et al., 1999). For instance, when using a 100 mm optical pathlength, the indicator dye induced pH_T perturbation is typically less than 0.006 pH_T units within the pH_T range of 7.6 to 8.0 (Chierici et al., 1999; Li et al., 2020; Table 1), which is relatively minor but not negligible. A common approach to account for this effect, as proposed by CB'93, involves performing a double addition of the indicator dye solution to the samples and calculating the difference in the resulting R values (ΔR) between the first (single) and second (double) addition. This ΔR correction is then applied to the measured R values. Alternatively, the correction can be expressed in terms of ΔpH_T , which may be directly applied to the computed pH_T values (Takeshita et al., 2020, 2022). Both ΔR and ΔpH_T correction approaches were evaluated. During each cruise, between two and four double indicator dye addition experiments were performed. In each experiment, seawater samples were modified to obtain four pH_T values ranging from 7.4 to 8.2, with four samples per pH_T level (N = 16 samples per experiment). Following blanking, an initial addition of 50 µL of mCP dye solution was made to each sample, and absorbance was measured as described in Section 2.2.2. A second addition of 50 µL of mCP dye solution was then made (resulting in a total of 100 µL of mCP dye solution added), and absorbance measurements were repeated. These double-addition experiments enabled the determination of linear regressions of the change in pH_T ($\Delta pH_T = pH_{T,2}$ - $pH_{T,1}$; where subscripts 2 and 1 refer to 100 μ L and 50 μ L of mCP dye solution added, respectively) or R (Δ R = R₂ - R₁) as a function of the initial $pH_{T,1}$ or R_1 , respectively (Supporting Information Fig. 1). The corresponding relationship was expressed as:

$$\Delta pH_T = a \cdot (pH_T - pH_T^{y=0})$$
 (5),

where a is the slope of the linear regression and $pH_T^{y=0}$ represents the pH_T at which the indicator dye addition has no effect. An analogous expression was used for ΔR [$\Delta R = a \cdot (R - R^{y=0})$, being a 'the particular slope for the ΔR -R linear regression]. Since the standard volume of mCP dye solution used in OVIDE-BOCATS cruises was 75 μ L, while the double addition experiments used 50 μ L additions, a correction factor of 75/50 was applied to adjust both ΔpH_T and ΔR . The corrected pH_T ($pH_{T,corrected}$) was thus calculated as:

$$pH_{T,corrected} = pH_m - 75/50 \cdot a \cdot (pH_m - pH_T^{y=0})$$
(6),

where pH_m is the uncorrected measured pH_T (i.e., prior to its ΔpH_T correction) [analogously: $R_{corrected} = R - 75/50 \cdot a' \cdot (R_m - R^{y=0})$]. If $pH_m > pH_T^{y=0}$, then $pH_{T,2}$ (or R_2) $< pH_{T,1}$ (or R_1), as the mCP dye addition lowers pH_m ; hence, $pH_{T,corrected}$ will be higher than pH_m . Conversely, if $pH_m < pH_T^{y=0}$, the mCP dye addition increases the pH_m , and $pH_{T,corrected}$ will be lower than pH_m .

The linear regressions of ΔR versus R_1 (ΔR -vs- R_1) and ΔpH_T versus $pH_{T,1}$ (ΔpH_T -vs- $pH_{T,1}$) obtained for each OVIDE-BOCATS cruise are summarized in Table 1. The slopes for ΔR -vs- R_1 range from 0.0048 (BOCATS2-2023 cruise) to 0.0230 (OVIDE-2006 cruise), with the perturbation vanishing ($\Delta R = 0$) when $R \approx 1.0 \pm 0.2$, i.e., when the sample pH_T closely matches that of the mCP dye solution. Carter et al. (2013) proposed a methodological refinement by normalizing ΔR with the change in absorbances at the isosbestic point ($\Delta_{488}A$; see Section 2.2.4), improving the robustness of the correction. Accordingly, using the Carter et al. (2013) approach [$\Delta (R/_{488}A)$ versus R_1 ; $\Delta (R/_{488}A)$ -vs- R_1] increased the overall explained variability (R^2) of the linear fits. Similarly, for ΔpH_T -vs- $pH_{T,1}$





regressions, the smallest slope was recorded for BOCATS2-2021 cruise and the largest again in the OVIDE-2006 cruise (Table 1). When using $\Delta(pH_T/_{488}A)$ -vs-pH_{T,1}, the distribution of regression slopes was similar but less variable (average regression: $-0.0431 \pm 0.019 \cdot (pH_T - 7.73 \pm 0.09)$; Table 1), consistent with the mCP dye perturbation trends reported by Takeshita et al. (2022) [$\Delta pH_T/\Delta_{488}A = -0.042 \pm 0.003 \cdot (pH_T - 7.76)$; N = 91]. The OVIDE-BOCATS pH_T data were corrected using the cruise-specific $\Delta pH_T/\Delta_{488}A$ relationships. Overall, the evaluation of the mCP dye's perturbation on the sample's pH_T was consistent across all cruises, regardless of whether ΔR - or ΔpH_T -based methods were used.

Table 1. Summary of each OVIDE-BOCATS cruise alias, the spectrophotometer used, and the mean and standard deviation of $_{488}$ A values (from 2002 to 2018 estimated using Eq. (7), from 2018 to 2023 directly measured). The table also includes the linear regression equations and their explained variance (R²) for the ΔR-vs-R₁, Δ (R/ $_{488}$ A)-vs-PH_{T,1} relationships. Additionally, it reports the corresponding Δ PH_T at pH_T = 7.7 and pH_T = 8.0, calculated using the Δ (pH_T/ $_{488}$ A)-vs-pH_{T,1} relationship for each cruise. Note that Δ R-vs-R₁ and Δ pH_T-vs-pH_{T,1} regressions are based on an addition of 50 μL mCP dye solution; therefore, a correction factor (e.g., 75/50) must be applied when using Δ R-vs-R₁ and Δ pH_T-vs-pH_{T,1} relationships to samples measured with a different addition volumes (e.g., 75 μL).

CRUISE	Spectrophotometer	488A	ΔR -vs- $R_1 \parallel R^2$	$\Delta(R/_{488}A)$ -vs- $R_1 R^2$	ΔpH_{T} -vs- $pH_{T,1} R^2$	$\Delta(pH_{T/488}A)$ -vs- $pH_{T,1} \parallel R^2$	ΔpH_T at ~7.7	ΔpH_T at ~8.0
Ovide-2002	CECIL-3041	0.331±0.020	-0.0068·(R-0.82) 0.32	-0.059·(R-1.07) 0.41	-0.0078·(pH _T -7.71) 0.51	-0.056·(pH _T -7.71) 0.59	0,000	0,005
Ovide-2004	Shimadzu UV- 2401PC	0.232±0.020	-0.0092·(R-0.96) 0.78	-0.038·(R-0.97) 0.81	-0.0078·(pH _T -7.70) 0.70	-0.033 · (pH _T -7.70) 0.73	0,000	0,002
Ovide-2006	Shimadzu UV- 2401PC	0.250±0.023	-0.035·(R-1.10) 0.92	-0.134·(R-1.00) 0.94	-0.023· (pH _T -7.70) 0.88	-0.103· (pH _T -7.68) 0.96	0,001	0,008
Ovide-2008	Shimadzu UV- 2401PC	0.230±0.015	-0.0060·(R-1.2) 0.60	-0.029·(R-1.04) 0.84	-0.0084·(pH _T -7.83) 0.89	-0.037·(pH _T -7.84) 0.89	-0,001	0,001
Ovide-2010	Shimadzu UV- 2401PC	0.233±0.015	-0.022·(R-1.06) 0.78	-0.096·(R-1.06) 0.81	-0.0106·(pH _T -7.68) 0.70	-0.069·(pH _T -7.68) 0.73	0,000	0,005
CATARINA-2012	Perkin Elmer Lambda 800 UV-VIS	0.211±0.016	-0.014·(R -0.80) 0.93	-0.100·(R -0.81) 0.94	-0.0090·(pH _T -7.55) 0.89	-0.065·(pH _T -7.58) 0.93	0,002	0,006
Geovide-2014	Shimadzu UV- 2401PC	0.218±0.007	-0.0066·(R -1.12) 0.76	-0.046·(R -1.16) 0.75	-0.0082·(pH _T -7.77) 0.76	-0.065·(pH _T -7.77) 0.71	-0,001	0,003
BOCATS-2016	Perkin Elmer Lambda 800 UV-VIS	0.369±0.022	-0.0070·(R-1.19) 0.81	-0.028·(R-1.19) 0.81	-0.0080·(pH _T -7.85) 0.91	-0.033·(pH _T -7.85) 0.91	-0,002	0,002
Ovide-2018	Shimadzu UV- 2401PC	0.358±0.027	-0.0137·(R-1.15) 0.8	-0.045·(R-1.04) 0.69	-0.0089·(pH _T - 7.76) 0.72	-0.030·(pH _T -7.76) 0.70	-0,001	0,003
BOCATS2-2021	Perkin Elmer Lambda 800 UV-VIS	0.359±0.027	-0.0070·(R-1.16) 0.96	-0.027·(R-1.16) 0.96	-0.0050·(pH _T - 7.76) 0.89	-0.021·(pH _T - 7.76) 0.90	0,000	0,002
BOCATS2-2023	Perkin Elmer Lambda 800 UV-VIS	0.389±0.032	-0.0048·(R-1.12) 0.92	-0.020·(R-1.12) 0.92	-0.0063·(pH _T - 7.80) 0.95	-0.023·(pH _T - 7.76) 0.96	-0,001	0,002

In addition to the impact of the mCP dye addition, both the ΔR and ΔpH_T corrections can be influenced by the performance characteristics of the spectrophotometer used (Carter et al., 2013; Álvarez et al., 2020; Takeshita et al., 2021; Fong et al., 2024). If the spectrophotometer follows the Beer-Lambert law (i.e., no optical non-linearity), the effect of the mCP dye addition results in a linear relationship for both ΔR -vs- R_1 and ΔpH_T -vs- $pH_{T,1}$ regressions (Li et al., 2020), meaning that the relationships are only affected by chemistry. This only-chemical effect was evaluated by Li et al. (2020) over a wide range of salinities and A_T s, including those present during OVIDE-BOCATS cruises, allowing us to replicate their chemical model (blue diamonds in Fig. 3). The ΔR -vs- R_1 regression exhibits better linearity than ΔpH_T -vs- $pH_{T,1}$ regression, though both reflect the mCP dye's interference in the physico-chemical ionic equilibrium of the marine carbonate system. However, when introducing a 0.04% deviation from linearity in the spectrophotometer (i.e., loss of the Beer-Lambert behavior, thus including an additional impact to the chemical effect) the regression slopes for both ΔpH_T -vs- $pH_{T,1}$ and ΔR -vs- R_1 roughly double, revealing that this instrumental non-linearity amplifies the chemistry effect of the mCP dye. Notably, while ΔpH_T remains linear during this distorsion, ΔR becomes non-linear (orange diamonds in Fig. 3). When R = 1 (i.e., $_{434}A = _{578}A$ and sample $pH_T = mCP$ dye pH_T), non-linearity impacts both absorbances equally, resulting in no change in R and therefore in



 pH_T . In contrast, deviations from R=1 (or $pH_T=7.65$) enhance this artifact due to increasingly unequal absorbances at $_{434}A$ and $_{578}A$, leading to spurious R values and biased pH_T .

These results suggest that the ΔpH_T -vs- $pH_{T,1}$ relationship provides a more accurate assessment of the mCP dye's effect on the sample's pH_T when the spectrophotometer exhibits even slight deviations from the Beer-Lambert law. Indeed, the small differences between the slopes of the ΔR -vs- R_1 and ΔpH_T -vs- $pH_{T,1}$ regressions reported in Table 1 can be attributed to the distinct ways in which pH_T and R respond to such nonlinearity. The theoretical slopes of ΔpH_T -vs- $pH_{T,1}$ shown in Fig. 3 are consistent with those derived experimentally (Table 1). The steepest experimental slopes observed during the cruises may reflect greater deviations from the Beer-Lambert law, which can depend on both the spectrophotometer used and the pH_T range of the seawater batches used in these assessments. Conversely, cruises with ΔpH_T -vs- $pH_{T,1}$ slopes closer to the chemical model prediction—such as in the 2021 and 2023 cruises—indicate better spectrophotometer performance. Nevertheless, the differences in $pH_{T,corrected}$ when applying either ΔR -vs- R_1 or ΔpH_T -vs- $pH_{T,1}$ corrections remain small (< 0.001 pH_T units; see Supporting Information Fig. 2), implying that the choice of correction method has minimal impact on the final estimation of the mCP dye perturbation. For consistency, OVIDE-BOCATS pH_T data were corrected using the $\Delta pH_T/\Delta_{488}A$ approach specific to each cruise.

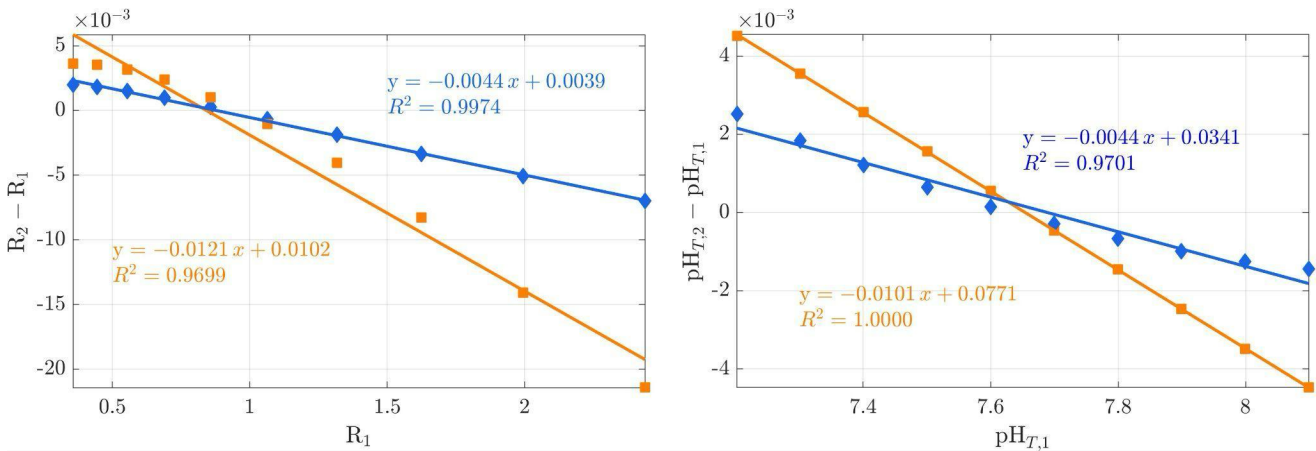


Figure 3. Theoretical evaluation of the difference of the impact of mCP dye perturbation on the sample's pH_T (S = 35; $A_T = 2300 \mu mol kg^{-1}$), depending on whether the spectrophotometer behaves linearly—i.e., follows the Beer-Lambert law—or not. The left and right panels depict the ΔR -vs- R_1 and ΔpH_T -vs-pH_{T,1} relationships, respectively. Blue diamonds represent an ideal, linear spectrophotometer response, derived from the chemical model of Li et al. (2020) based on single and double additions of 50 μL of mCP dye solution ([2 mM]) to a 28 mL sample cell with a 10 cm pathlength ($_{488}A = 0.242$), assuming a pH_T of the mCP dye solution of 7.65). Orange squares incorporate an attenuation factor of 0.04% to simulate a deviation from linearity, thus representing the combined effect of spectrophotometer non-linearity and perturbation in the physico-chemical ionic equilibrium

2.2.4 Absorbance at the isosbestic point

During the OVIDE-BOCATS cruises, mCP dye was manually added to samples using an adjustable repeater pipette (see Section 2.2.2). Manual addition introduced volume deviations exceeding 20% in approximately 3% of the samples (~ 706 cases), potentially affecting ΔR and ΔpH_T determinations. To address variability in the volume of mCP dye solution added, Carter et al. (2013) recommended measuring absorbance at the isosbestic point (488A),





which provides a reliable proxy for actual mCP dye concentration in the sample cell. Accurate quantification of the mCP dye concentration is particularly important when applying the DB'17 methodology for impurity correction, since the 434A_{imp} value is directly proportional to the mCP dye content. Therefore, sample-specific estimates of mCP dye concentration via 488A allow for a more precise estimate of the 434A_{imp} value.

Since 2018, OVIDE-BOCATS cruises have incorporated measurements at $_{488}$ A following the recommendation by Carter et al. (2013). The additions of 75 µL of 2 mM mCP dye solution to 28 mL seawater sample resulted in averaged $_{488}$ A values of 0.359 ± 0.027 (N = 2,193), 0.358 ± 0.027 (N = 2,154), and 0.377 ± 0.032 (N = 2,342) during the 2018, 2021, and 2023 cruises, respectively. These averages were not statistically different from one another, resulting in a $_{488}$ A mean value of 0.370 ± 0.033 for the period 2018—2023. This $_{488}$ A mean value was used to derive a parameterization for estimating $_{488}$ A from R values, fitted for an mCP dye concentration in the cell of 5.36 µM—particularly useful for pre-2018 cruises, where $_{488}$ A was not measured. For these earlier cruises, $_{488}$ A was estimated using the following parameterization:

$$_{488}A = _{578}A \cdot (-2.5486 R^{2.5} + 17.338 R^2 - 46.779 R^{1.5} + 63.109 R - 43.393 R^{0.5} + 12.962)$$
 (7).

This fit, based on 6,910 samples from the 2018, 2021, and 2023 cruises (Supporting Information Fig. 3), explained 98.9% of the variance ($R^2 = 0.989$) and reproduces $_{488}A$ with a mean error of 0.002 ± 0.010 . It enabled a more accurate estimation of mCP dye concentrations across all cruises and improved the assessment of mCP dye impurity effects on $_{434}A$ (see Sect. 3.4). Additionally, it enhanced the accuracy of mCP dye perturbation corrections using $\Delta R/_{488}A$ and $\Delta pH_T/_{488}A$ (Table 1). A simplified parameterization using $_{434}A$ (e.g., $_{434}A = -0.0747 \cdot R + 0.403$ for 3.3 μM mCP dye concentration in the sample cell) is possible, but requires correction for $_{434}A_{imp}$.

2.2.5 pH_T measurement repeatability

Throughout the 11 OVIDE-BOCATS cruises, a total of 502 duplicate samples were collected to evaluate the reproducibility of pH_T measurements using an impure mCP dye. At selected stations, two Niskin bottles were closed at the same depth to obtain replicates. Figure 4 displays the absolute pH_T differences between replicates for each cruise. The overall mean and standard deviation of these differences is 0.0014 ± 0.0015 pH_T units (N = 502). The highest reproducibility was obtained in 2021, with 92 duplicate samples yielding a mean difference of 0.0007 ± 0.0010 pH_T units. This improved reproducibility, particularly evident during the two most recent cruises, coincides with more precise evaluations of mCP dye effects (Table 1) and likely reflects the better performance of the spectrophotometer used (PerkinElmer Lambda 800; Table 1), contributing to the overall improvement in data quality. Typical reproducibility across OVIDE-BOCATS cruises ranged between 0.0007 and 0.0018 pH_T units.

3. Assessment of the effect of indicator dye impurities on pH_T

During the OVIDE-2018, BOCATS2-2021, and BOCATS2-2023 cruises, paired measurements were performed in duplicate samples collected from the same Niskin bottle and measured using two types of mCP dye: (i) purified mCP, provided by Dr. Byrne's laboratory, University of South Florida, USA (FB6 batch), and (ii) unpurified mCP, commercially available from Sigma-Aldrich (Cat. No. 211761-5G, batch #07005HH). pH_T values were obtained applying the L'11 parametrization to R values obtained with purified mCP dye, and the CB'93 parametrization combined with the DVD'98 correction (CB'93+DVD'98 hereafter) to R values obtained with unpurified mCP dye.





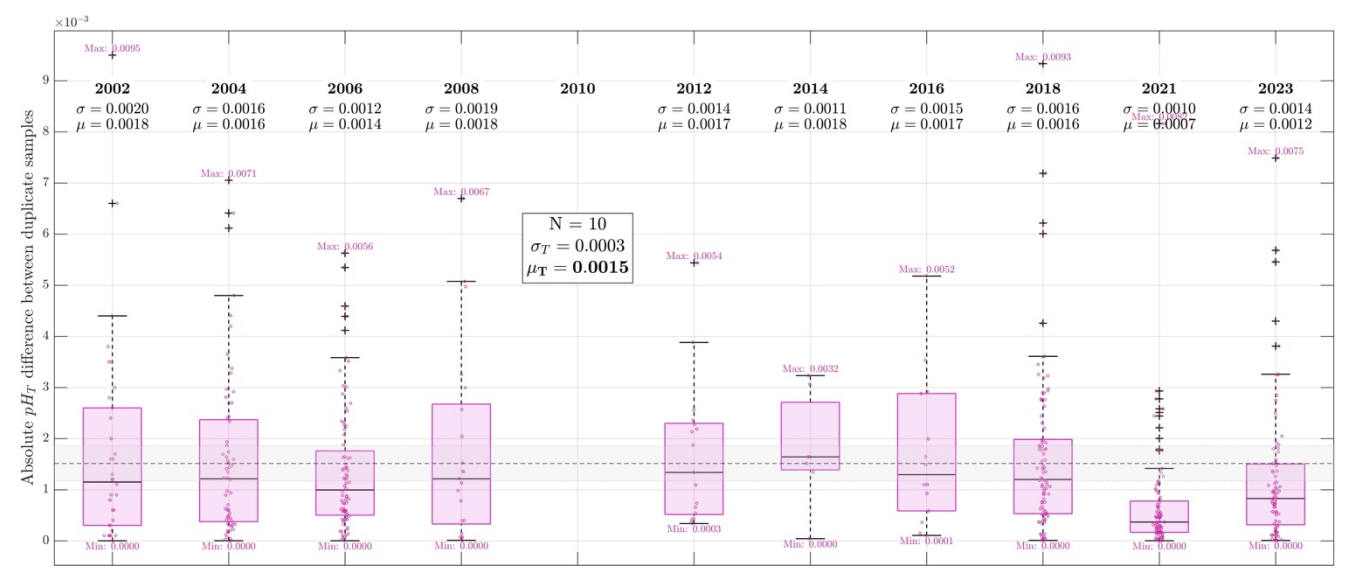


Figure 4. Whisker boxplots showing pH_T repeatability across OVIDE-BOCATS cruises (2002—2023), represented as the absolute difference between duplicate samples collected during each cruise. The number of duplicate samples analyzed per cruise were: 34 (2002), 64 (2004), 84 (2006), 21 (2008), 0 (2010), 17 (2012), 7 (2014), 14 (2016), 90 (2018), 92 (2021), and 79 (2023). For each cruise, the subset mean (μ) and standard deviation (σ) are indicated, as well as the minimum and maximum values. The overall mean (μ _T) and standard deviation (σ _T) across all 10 cruises are shown in the inset textbox. μ _T is also plotted as a horizontal dashed line, with σ _T represented as a shaded gray band. Each boxplot displays the median (horizontal line), first (Q1) and third (Q3) quartiles (box edges), and the minimum and maximum within 1.5 times the interquartile range (IQR = Q3 – Q1) (whiskers).

3.1 TRIS buffer validation

TRIS buffers in synthetic seawater (batch numbers 30 and 40) were obtained from Prof. Dickson's laboratory (Scripps Institution of Oceanography; USA). These buffers were supplied in 125 mL borosilicate glass bottles and contained an equimolar mixture of *TRIS/TRIS*-HCl in a synthetic seawater of nominal salinity 35. The reference pH_T values of these batches can be calculated following DVD'98. Multiple bottles from both batches were measured during the BOCATS2-2021 and BOCATS2-2023 cruises using two mCP dye solutions: (i) unpurified mCP (75 μL of 2 mM solution; Sigma-Aldrich), and (ii) purified mCP (10 μL of 11 mM solution; provided by Prof. R. Byrne's laboratory).

Each buffer sample was measured in quadruplicate. Following blank measurement, the sample was placed in the spectrophotometer's thermostated cell holder and allowed to equilibrate for 10-15 minutes. Measurements were then conducted at 3-minute intervals. To ensure full thermal stabilization, only the last two measurements out of the four were retained for analysis. Temperature at the end of the fourth measurement was recorded using a calibrated Physics 100-1 thermometer, with an uncertainty of ± 0.01 °C.

A total of 16 measurements performed using Sigma-Aldrich unpurified mCP dye, following the OVIDE-BOCATS protocol (CB'93+DVD'98; see Sect. 2.2.2), showed a consistent positive bias of 0.0105 ± 0.0013 pH_T units relative to the nominal *TRIS* pH_T values (Fig. 5). In contrast, 15 measurements conducted with the purified mCP dye, applying the L'11 parameterization, yielded values that were tightly centered around the nominal *TRIS* pH_T values, with a negligible bias of -0.0003 ± 0.0011 pH_T units. No Δ R or Δ pH_T corrections were applied to either dataset, as

the buffer capacity of TRIS is approximately 20 times higher than that of seawater, rendering the impact of the mCP dye addition on pH_T negligible.

The correction of $_{434}A_{imp}$ due to mCP dye impurities, as proposed by DB'17, was evaluated using a value of $_{434}A_{imp}$ = 0.004413 absorbance units (given in their Table 2 for Sigma-Aldrich lot #11517KC at a mCP dye concentration of 3.3 μ M in the seawater sample). Applying this correction enabled the use of the L'11 parameterization, substantially reducing the observed difference with purified mCP dye measurements to 0.0020 ± 0.0013 pH_T units. Recognizing that impurities can vary between batches of the same mCP dye brand, a second test using $_{434}A_{imp} = 0.0034$ absorbance units, consistent with that obtained by Álvarez et al. (submitted), further reduced the offset to -0.0005 ± 0.0013 pH_T units.

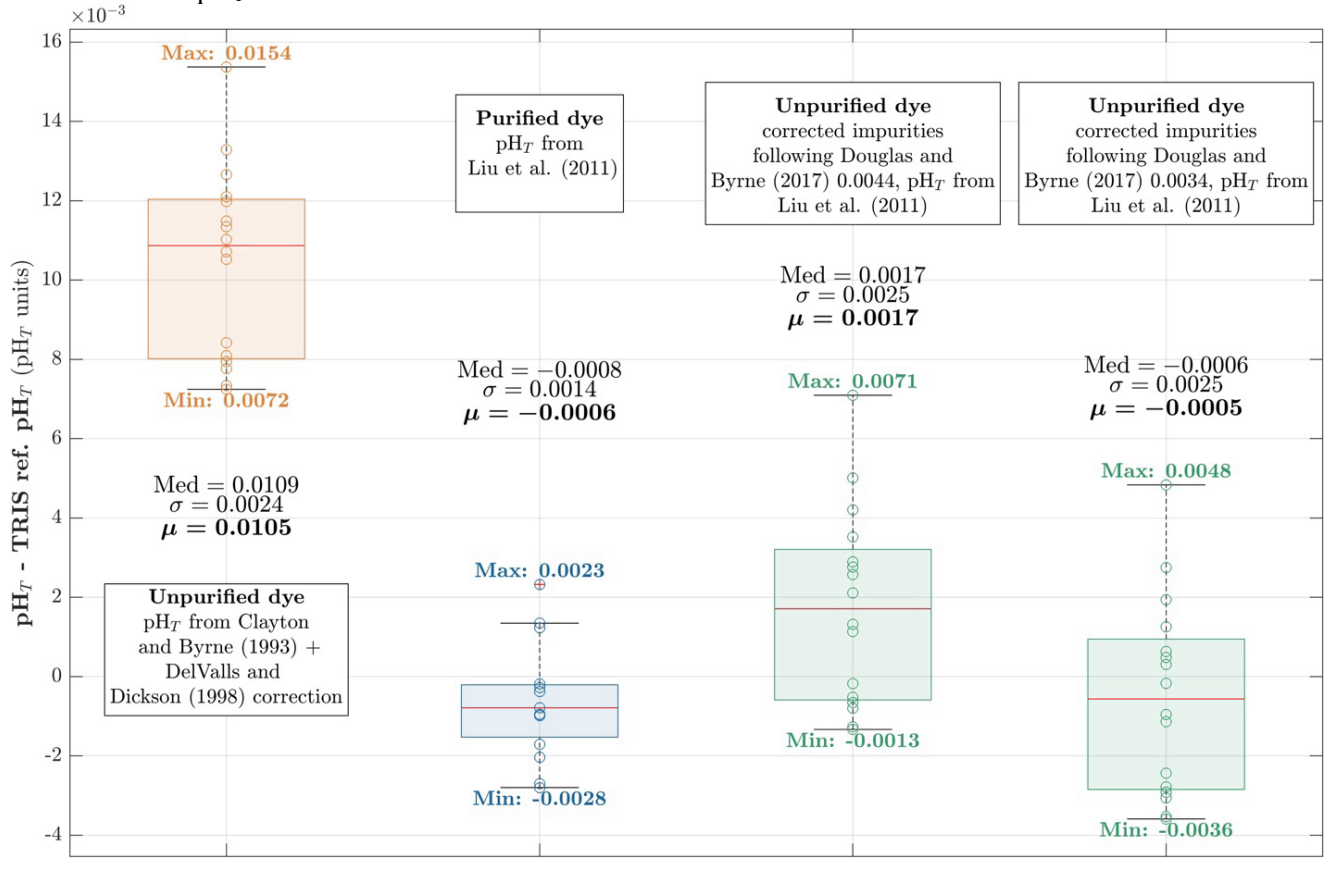


Figure 5. Whisker boxplots of pH_T differences relative to *TRIS* buffer reference values, comparing results obtained using purified and unpurified mCP dyes. Each boxplot represents a different calculation approach: the orange boxplot shows pH_T computed using unpurified mCP dye with the CB'93 parameterization and DVD'98 correction (N = 16); the blue boxplot shows pH_T computed using purified mCP dye with the L'11 parameterization (N = 15); and green boxplots show pH_T computed using unpurified mCP dye corrected for impurities using the DB'17 methodology with $_{434}A_{imp} = 0.0044$ and $_{434}A_{imp} = 0.0034$ absorbance units, respectively, and pH_T then calculated using the L'11 parameterization. Within each boxplot, the red line indicates the median (*Med*), the box edges denote the first and third quartiles, and whiskers extend to data points within 1.5 times the interquartile range. Mean (μ) and standard deviation (σ) values are provided for each subset, and the minimum and maximum values are indicated.

https://doi.org/10.5194/essd-2025-476 Preprint. Discussion started: 20 October 2025 © Author(s) 2025. CC BY 4.0 License.





3.2 Duplicate measurements of natural seawater

During the 2021 cruise, six duplicate pH_T samples were collected at each hydrographic station along the OVIDE-BOCATS transect, with sampling points carefully distributed throughout the water column to represent different water masses. In addition to the routine pH_T determinations conducted according to the OVIDE-BOCATS protocol (i.e., addition of 75 μL of Sigma-Aldrich [2 mM] mCP dye solution and pH_T computed using CB'93+DVD'98; see Sect. 2.2.2), these six replicate samples per profile were also measured using purified mCP dye (10 µL of [11 mM] mCP dye supplied by Dr. Byrne's laboratory, and pH_T determined using the L'11 parameterization).

464 465 466

467

468

469

470

458

459

460

461

462

463

These duplicate measurements encompassed the full pH_T range typically observed during OVIDE-BOCATS cruises (7.7 to 8.0 pH_T units). As shown in Fig. 6, the standard OVIDE-BOCATS procedure yields pH_T values that are, on average, 0.0113 ± 0.0017 (N = 176) pH_T units higher than those obtained using the purified mCP dye and the L'11 parameterization. These results align with the findings from the TRIS buffer experiments (see Sect. 3.1). The differences between the two methods showed no significant dependence on pH_T (Fig. 7, green dots), in agreement with the theoretical expectation illustrated in Fig. 2 (blue line, Aldrich-3.4).

471 472 473

474

475

476

477

478

479

480

481

482

483

484

485

486

487

489

491

493

494

When the DB'17 methodology was applied using a $_{434}A_{imp}$ value of 0.004413 absorbance units at $_{488}A = 0.225$, the offset was reduced to 0.0015 ± 0.0017 pH_T units—statistically indistinguishable from zero. Using a $_{434}A_{imp}$ value of 0.0034 absorbance units further minimized the offset to -0.0001 ± 0.0017 pH_T units, corroborating the impurity correction results from the TRIS buffer experiment. The individual 434A_{imp} values applied here are proportionally dependent on the 488A in each measurement.

3.3 Duplicate measurements of modified seawater

During the OVIDE-2018 cruise, surface seawater with a salinity of 35.7 was treated using HCl or Na₂CO₃ to produce four distinct pH_T levels (7.45, 7.70, 7.95, and 8.19). These were stored in separate Niskin bottles and sampled using the same protocol as for natural seawater. For each batch, four to six samples were analyzed for pH_T using the standard OVIDE-BOCATS procedure (CB'93+DVD'98 and 75 µL of unpurified Sigma-Aldrich mCP dye [2 mM] solution added to the cell), and an equivalent number was measured using purified mCP dye (75 µL of mCP dye [2.5 mM] solution added to the cell, FB5-2017 from Dr. Byrne's laboratory and the L'11 parametrization). This experiment extends the comparison conducted with TRIS buffer and natural seawater to a wider pH_T range, representative of conditions encountered in the South Atlantic and Pacific Oceans.

The mean pH_T offset between the two methods (measuring with unpurified mCP dye and applying CB'93+DVD'98 488 versus purified mCP dye and applying the L'11 parameterization) across 22 measurements was 0.0109 ± 0.0011 pH_T units, consistent with previous results from TRIS and natural seawater duplicate samples (Sect. 3.1 and Sect. 490 3.2). No significant trend was observed across the pH_T range (Fig. 7, regression p-level > 0.05). Similarly, differences observed in natural seawater (green dots in Fig. 7) also showed no significant correlation with pH_T 492 (slope = -0.000 ± 0.002 ; p-level > 0.05). Furthermore, the magnitude and behavior of the observed differences are consistent with theoretical expectations (Fig. 2, yellow line), assuming a 434A_{imp} value of 0.0034 absorbance units for Sigma-Aldrich mCP dye at a final concentration in the cell of 3.3 μM (as per Table 2 of DB'17).



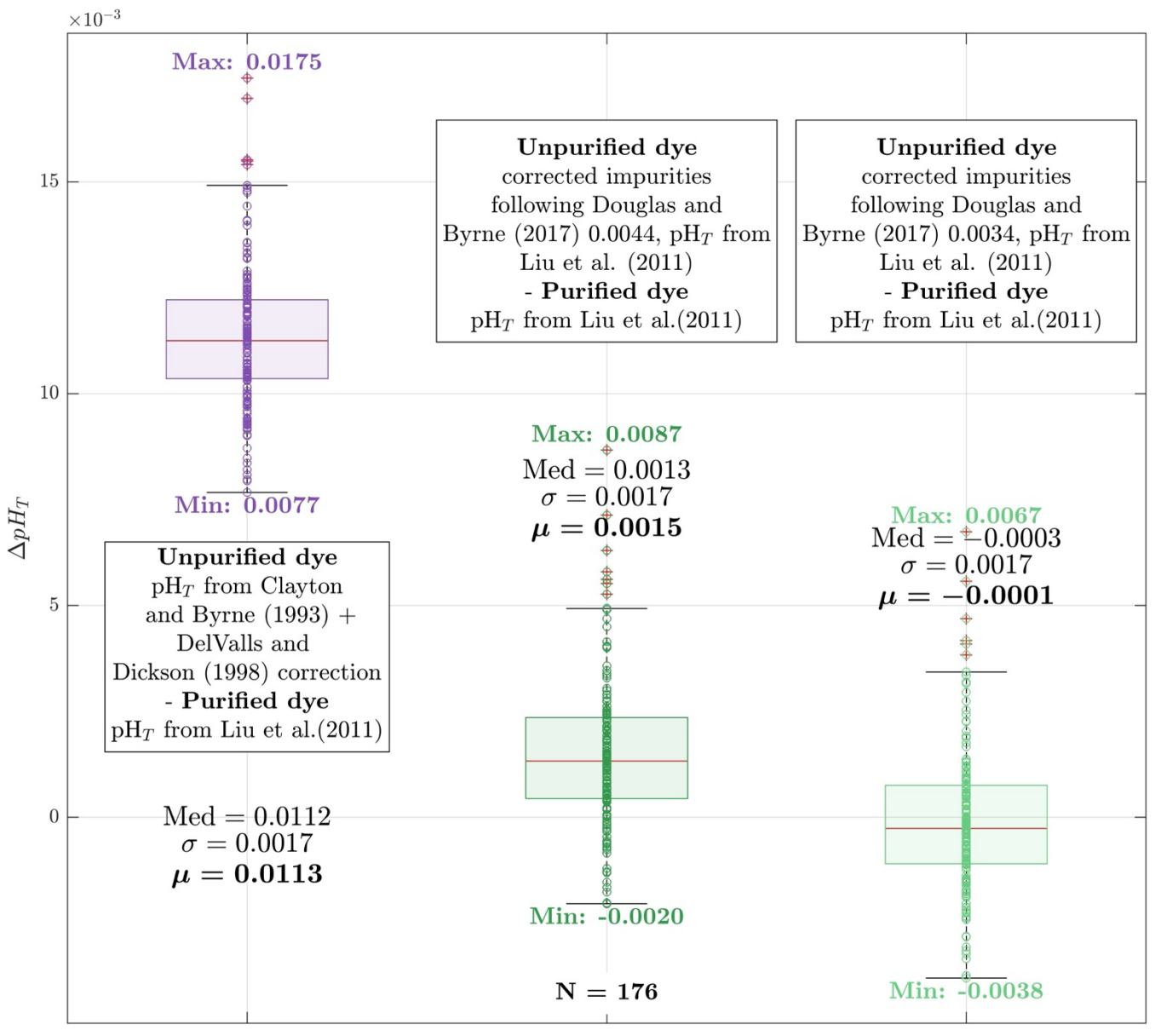


Figure 6. Whisker boxplots showing pH_T differences between duplicate samples measured using purified and unpurified mCP dyes (N = 176). *Med* indicates the median (red line inside each box), σ the standard deviation, and μ the mean of each subset. The minimum and maximum values are also indicated. The first boxplot (purple) shows the pH_T difference between measurements using unpurified mCP dye (pH_T calculated with CB'93+DVD'98) and purified mCP dye (pH_T calculated with L'11 parametrization). The second boxplot (first green) shows differences after applying the DB'17 correction to R values obtained with unpurified mCP dye, using $_{434}A_{imp} = 0.0044$ absorbance units, followed by pH_T computation with L'11 parametrization. The third boxplot (second green) applies the same procedure but with $_{434}A_{imp} = 0.0034$ absorbance units.





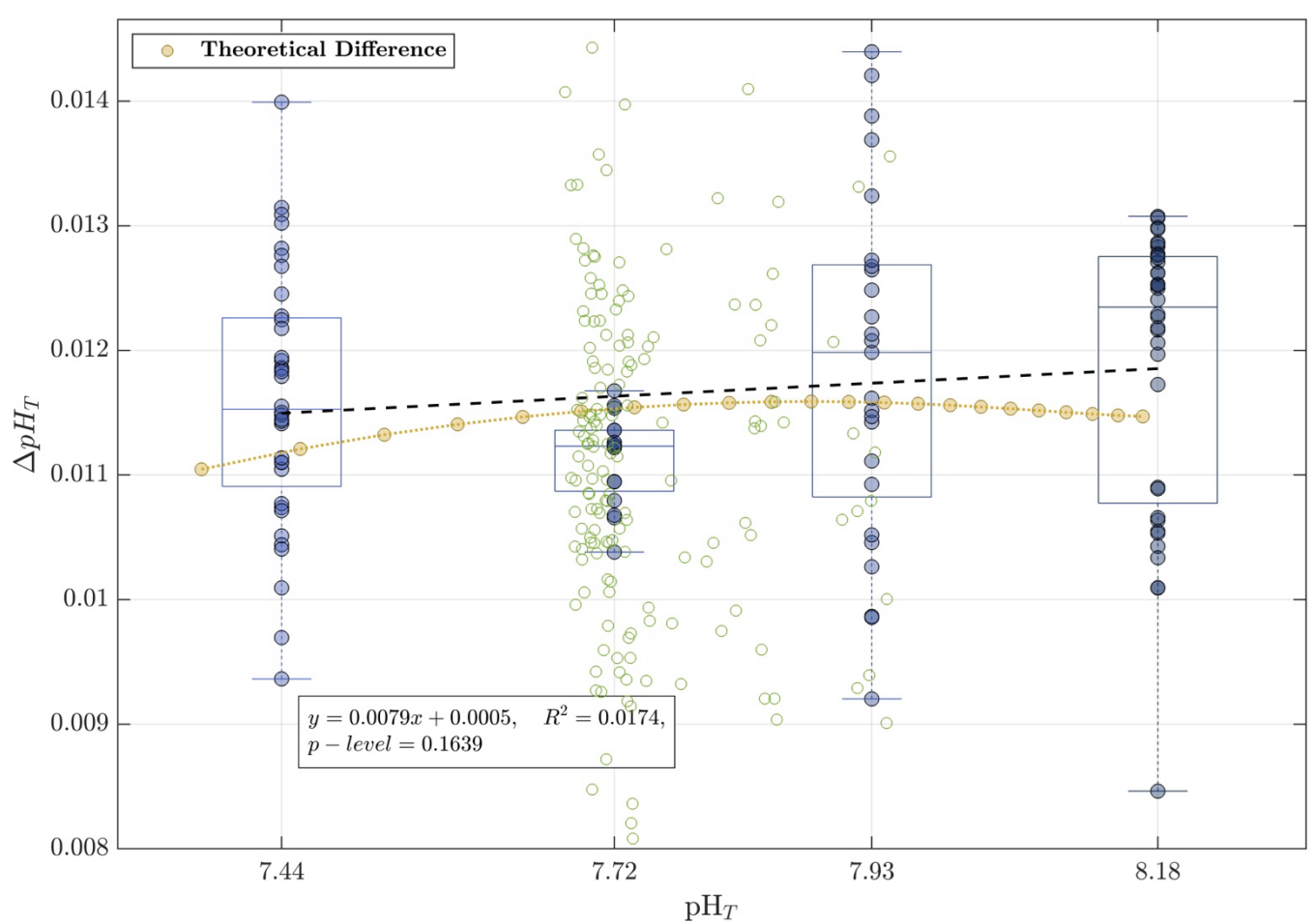


Figure 7. Differences in pH_T measurements between replicate samples measured using unpurified mCP dye (CB'93+DVD'98) and purified mCP dye (L'11 parameterization) across four pH_T levels obtained from modified seawater experiments. The black dashed line shows the linear regression of the differences as a function of pH_T , with regression statistics summarized in the inset box. The yellow line represents the expected pH_T differences assuming a $_{434}A_{imp}$ value of 0.034 absorbance units, as modeled in Fig. 2. Green dots correspond to the 176 individual pH_T differences presented in the first (purple) boxplot of Fig. 6.

3.4 pH_T correction

DB'17 proposed a value of $_{434}A_{imp} = 0.004413$ absorbance units for a Sigma-Aldrich mCP dye at a final concentration of 3.3 μ M in the sample cell ($_{488}A = 0.225$; Takeshita et al., 2021). However, based on our experimental results, we found that a better fit under our conditions corresponded to a $_{434}A_{imp}$ value of 0.0034 absorbance units. Given that $_{434}A_{imp}$ is proportional to $_{488}A$, which in turn reflects the final mCP dye concentration in the cell, we derived the following relationship:

$$_{434}A_{imp} = 0.0034 / 0.2250 \cdot _{488}A = 0.0151 \cdot _{488}A$$
 (8).

Accordingly, the impurity correction was applied to each sample by subtracting the computed $_{434}A_{imp}$ (Eq. 8) from the sample measured $_{434}A$, yielding:





$$434A_{\text{corr,pur}} = 434A - 434A_{\text{imp}} = 434A - (0.0151 \cdot 488A)$$
 (9),

$$R_{corr,pur} = (_{578}A - _{730}A) / (_{434}A_{corr,pur} - _{730}A)$$
 (10),

where 434A_{corr,pur} is the corrected 434A, and R_{corr,pur} corresponds to the R value as if measured with a purified mCP dye. Subsequently, pH_T was recalculated using the L'11 parameterization.

Implementing this correction required a comprehensive recovery and reassessment of historical $_{434}$ A, $_{578}$ A, and $_{488}$ A values dating back to the 2002 cruise. Note that for data prior to 2018, $_{488}$ A values were estimated from Eq. (7). While corrections related to the mCP dye addition effect were included in the data published in GLODAPv2.2023 (Lauvset et al., 2024), the $_{488}$ A-based correction described in Sect. 2.2.3 had not yet been incorporated. Final pH_T values included in this work were computed from the corrected absorbance data, using the recalculated R_{corr,pur}, along with the updated mCP dye perturbation correction $\Delta(pH_T/_{488}A)$ -vs-pH_{T,1}.

4. Results and Discussion

4.1 Database product

We present a new database comprising 23,535 seawater samples with spectrophotometric pH_T values, each accompanied by complete spatiotemporal metadata–including latitude, longitude, pressure, depth, date, and time—as well as in situ measurements of temperature, salinity, and dissolved oxygen. Dissolved oxygen concentrations were primarily determined using the Winkler titration method; where unavailable or deemed unreliable, values from a calibrated oxygen sensor mounted on the *Conductivity, Temperature, and Depth* (CTD) instrument were used. The dataset incorporates a quality flagging scheme consistent with GLODAPv2 recommendations (Key et al., 2015; Olsen et al., 2016), where flag 2 denotes good data, 3 and 4 indicate questionable and bad data, respectively, and 9 denotes not measured. Specifically, 71 pH_T values were flagged as questionable (flag = 3).

Spectrophotometric pH_T data collected between 2002 and 2018 were computed using the CB'93 parameterization with the DVD'98 correction (+0.0047 pH_T units), and were already available in the GLODAPv2.2023 release (Lauvset et al., 2024). The newly compiled pH_T dataset presented here significantly extends the temporal coverage by including pH_T measurements from the 2021 and 2023 cruises, which were not previously available. In addition, for the first time, associated absorbance readings (434A, 578A, and 488A) are provided alongside pH_T values. This comprehensive and corrected pH_T dataset provides a robust foundation for future reassessments, such as the application of updated absorbance-to-pH_T parameterizations or transformations to alternative pH scales (e.g., the "free" hydrogen ion scale).

4.2 Consistency of the pH_T correction

The differences between the former-procedure—applying the CB'93 parameterization with the DVD'98 correction to R values derived from unpurified mCP dye—and the updated method presented here—applying the L'11 parameterization to R values derived from unpurified mCP dye corrected for the impurity effect (see Sect. 3.4)—are, on average, $+0.011 \pm 0.002$ (1σ) pH_T units (N = 23,535; Supporting Information Fig. 4), in line with results from the assessment experiments described in Section 3. These differences show a slight negative correlation with pH_T, with smaller offsets observed at higher pH_T values (Supporting Information Fig. 4). The slopes of the linear regressions of these differences versus pH_T range from -0.0064 ± 0.0001 to 0.0005 ± 0.0001 pH_T units. It should be noted that this range is comparable in magnitude to other uncertainty sources—such as the effect of the addition



of mCP dye to the sample pH_T , and the instrumental measurement uncertainty (e.g., Sect. 2.2.3)—which may contribute to the overall variability in the observed differences.

To assess the internal consistency and long-term comparability of the corrected pH_T values, we examined the deep layer of the Iberian Basin, associated with the North East Atlantic Deep Water (NEADW). This layer has been recognized as a stable reference for the OVIDE-BOCATS program, as its properties show minimal long-term variability (García-Ibáñez et al., 2016). Supporting this minimal variability, Steinfeldt et al. (2024) reported no detectable accumulation of anthropogenic CO₂ in this layer based on chlorofluorocarbons measurements.

The average pH_T in the NEADW layer over 11 cruises (2002–2023) was 7.7314 \pm 0.0015 (1 standard deviation; 1σ), with only two cruises (2008 and 2018) exceeding the mean by more than 1 standard deviation (Fig. 8). The standard deviation within individual cruises was generally low (< 0.0018 pH_T units), with the exception of the 2004 cruise (0.0022 pH_T units). Additionally, the cruise-specific mean pH_T values showed no correlation with the difference between the old and new pH_T values (Supporting Information Fig. 5). These findings reinforce the reliability of the applied correction for the effects of impurities in the Sigma-Aldrich mCP dye (Sect. 3.4), based on a $_{434}A_{imp}$ value of 0.0034 ± 0.0010 absorbance units for $_{488}A = 0.225$.

However, it is important to acknowledge a limitation: the $_{434}A_{imp}$ value was not directly determined for each individual batch of mCP dye, as recommended by DB'17. In practice, this is challenging—especially for older cruises—since the specific mCP dye batches may no longer be available. While Sigma-Aldrich mCP dye batches have been shown to have a narrow impurity range (typically > 90% purity; Álvarez et al., submitted), variations between batches still exist. Thus, assuming a single correction value ($_{434}A_{imp} = 0.0034$) across all cruises could be questioned. We conservatively estimate an absorbance uncertainty of ± 0.001 due to batch variability, which translates to an uncertainty of approximately ± 0.002 pH_T units. The estimate is consistent with the inter-cruise variability observed (Fig. 8), supporting the use of $_{434}A_{imp} = 0.0034$ as a reasonable and robust correction value for the entire OVIDE-BOCATS dataset.

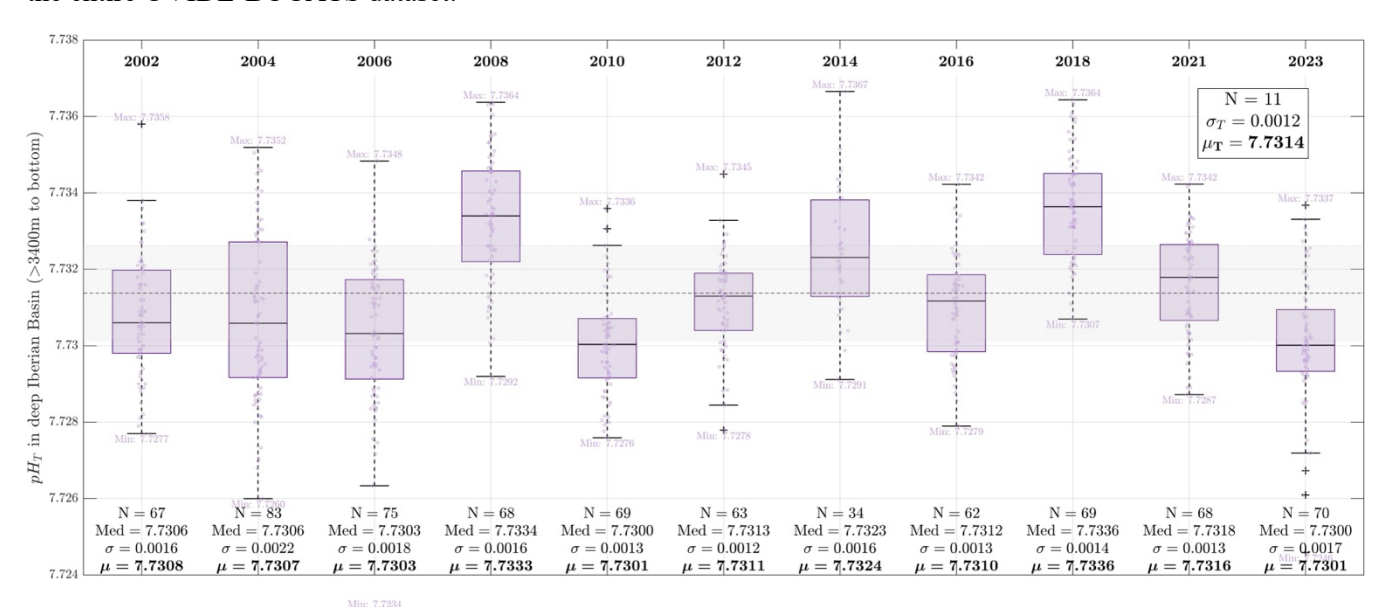


Figure 8. Variability of pH_T in the lower NEADW (deep Iberian Basin, observations > 3,400 m and east of 15.45°W) during the 11 OVIDE-BOCATS cruises. These data are used to assess the internal consistency of pH_T measurements over time. N refers to the number of samples analyzed in each cruise; Med indicates the median pH_T

https://doi.org/10.5194/essd-2025-476 Preprint. Discussion started: 20 October 2025 © Author(s) 2025. CC BY 4.0 License.



96



of each subset (shown as a black line within each boxplot); σ is the standard deviation; and μ is the mean. Minimum and maximum values are also shown for each cruise. The overall mean (μ_T; dashed horizontal line) and standard deviation (σ_T; shaded gray band) across all 11 cruises are provided in the up-right inset.

4.3 Implications of the pH_T correction on OA and aragonite saturation horizon

The correction applied to our pH_T dataset—an approximately constant offset across cruises—has negligible implications for previously reported OA rates by García-Ibáñez et al. (2016) and Fontela et al. (2020a). However, it does affect the calculation of the aragonite saturation, particularly the saturation horizon depth estimated by Pérez et al. (2018) and García-Ibáñez et al. (2021). To assess this impact, aragonite saturation horizons were recalculated using in situ temperature, salinity, A_T, and pH_T values, both before and after correcting for 434A_{imp} (see Sect. 3.4), using the carbonate chemistry constants from Lueker et al. (2000) and the boron formulation of Lee et al. (2010).

This reevaluation reveals a more pronounced reduction in aragonite saturation at the surface (from -0.040 to -0.065), which progressively diminishes with depth, reaching changes of -0.016 near the seafloor. Although changes at depth appear small in absolute terms, the weak vertical gradient in aragonite saturation in deeper layers translates into a significant vertical shift in the saturation horizon—rising by approximately 120 m to 200 m. For instance, in the NA subpolar gyre, where the aragonite saturation horizon currently resides near 2,700 m depth, the revised (lower) pH_T values shift it upward by approximately 150 m. This shift implies that vulnerable cold-water coral ecosystems may be exposed to undersaturation conditions in shallower and more extensive regions than previously estimated. This reassessment underscores the importance of accurate pH_T determinations: even subtle biases can propagate into substantial differences in projected impacts on sensitive deep-sea habitats.

To investigate the spatial and temporal evolution of pH_T along the OVIDE-BOCATS section, observations from the new OVIDE-BOCATS database were interpolated onto a common 7 km x 1 dbar grid. Each cruise's station positions were projected onto the grid by identifying the closest grid node (minimum distance), followed by linear interpolations using a Delaunay Triangulation approach (Amidror, 2002). This method ensured optimal station overlap while preserving dataset consistency across years.

Figure 9 displays the pH_T distributions from the 11 cruises (2002–2023), along with the overall mean distribution. Surface waters show the highest pH_T values, particularly along the eastern boundary, where elevated temperatures (not shown) partly contribute to the increase. Minimum pH_T values generally occur in intermediate waters (\sim 500–1,500 m), except in the Iberian Basin, where the presence of Mediterranean Water–characterized by a warm, saline core at \sim 1,000 m–causes a downward shift of the pH_T minimum to \sim 2,000 m.

Notably, a persistent pH_T minimum appears in the Iceland Basin between 500 m and 1,000 m, associated with intermediate waters with high Apparent Oxygen Utilization (AOU; Supporting Information Fig. 6a). This layer, influenced by older water masses transported by the North Atlantic Current (NAC) and exhibiting elevated remineralization rates (de la Paz et al., 2017), has shown significant spatial expansion over time. Since 2016, waters with pH_T below 7.71 have progressively expanded eastward, deepening toward \sim 2,000 m and reaching the Azores-Biscay Ridge (see Fig. 1 for georeference). In addition, the low-pH_T layer has spread into the Irminger Basin since 2010.



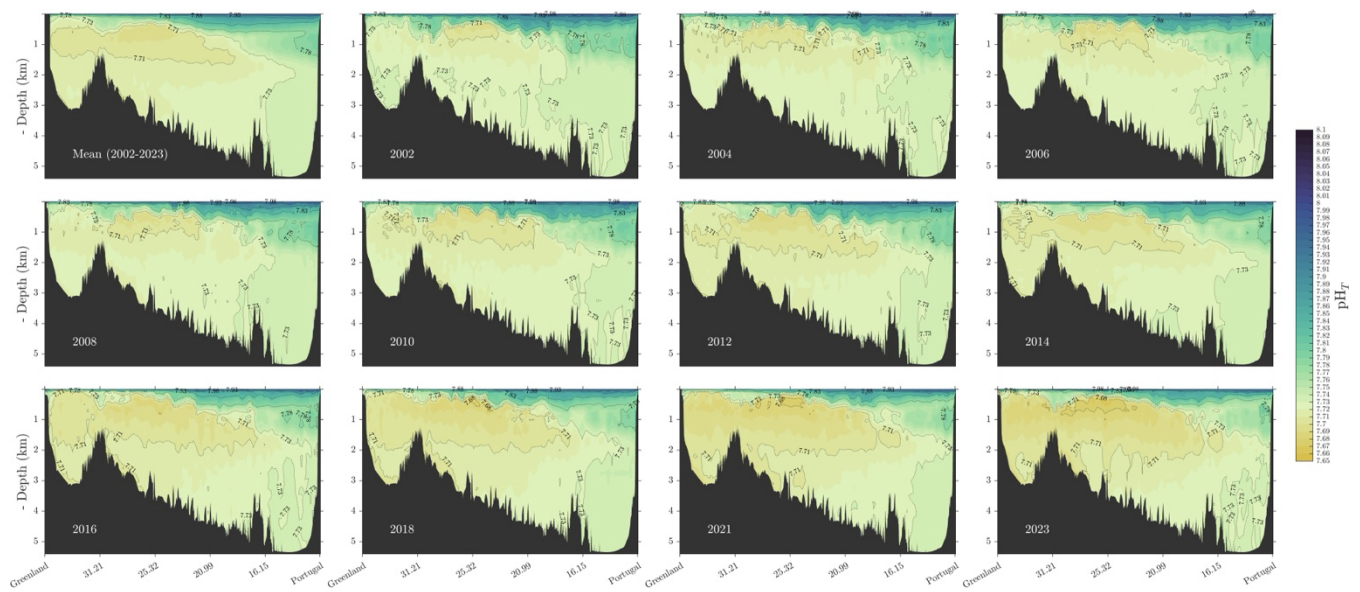


Figure 9. Distribution of pH_T normalized to 25°C and 1 atm along the OVIDE-BOCATS section (Fig. 1) for each cruise from 2002 to 2023, as well as the overall mean of all 11 OVIDE-BOCATS cruises. The section is plotted with longitudes (°W) in the x-axis.

In the Irminger Basin, a subsurface pH_T minimum (< 7.73) was already evident in 2002, associated with DSOW. This signal reappeared in 2014 with even lower values (< 7.70) and has progressively thickened through to the most recent observations in 2023. Although less intense than the DSOW signal, ISOW in the Iceland Basin has also shown a noticeable OA signal since 2016, reaching comparable pH_T values to those found in DSOW. In contrast, the deep pH_T maximum observed in 2002 at depths of 2,700—3,000 m—extending eastward from 20°W—had largely disappeared by 2010, becoming confined to the Iberian Basin. There, maximum pH_T values persist between 3,000 and 5,250 m depth, corresponding to the core of NEADW.

This contrast in deep-ocean pH_T between the more recently ventilated waters of the Irminger and Iceland Basins and the older, more stable NEADW is consistent with differential exposure to C_{ant} . Waters in the subpolar basins—having had more recent contact with the atmosphere or mixed with recently ventilated layers—have absorbed more C_{ant} , leading to their enhanced OA (Fig. 10) (García-Ibáñez et al., 2016).

DSOW exhibits a particularly strong OA (rate < -0.0015 pH $_T$ yr $^{-1}$), extending along the bottom of the Irminger Basin. A similar, though less intense, signal is seen in ISOW (< -0.0010 pH $_T$ yr $^{-1}$). The highest OA rates (< -0.002 pH $_T$ yr $^{-1}$) are observed in the surface layers (0—500 m) due to direct air-sea CO $_2$ exchange. These upper layers also exhibit high interannual pH $_T$ variability (Fig. 10), which correlates negatively with AOU (Supporting Information Fig. 6b). This pH $_T$ -AOU relationship suggests a strong influence of mesoscale variability, particularly associated with the NAC, which is known for its energetic and variable meandering in this region (Daniault et al., 2016). As a result, OA rates in NAC-influenced areas may be either enhanced or masked by spatial variability of the natural component in the pH $_T$ variability, sometimes leading to non-significant OA rates despite ongoing Cant uptake.



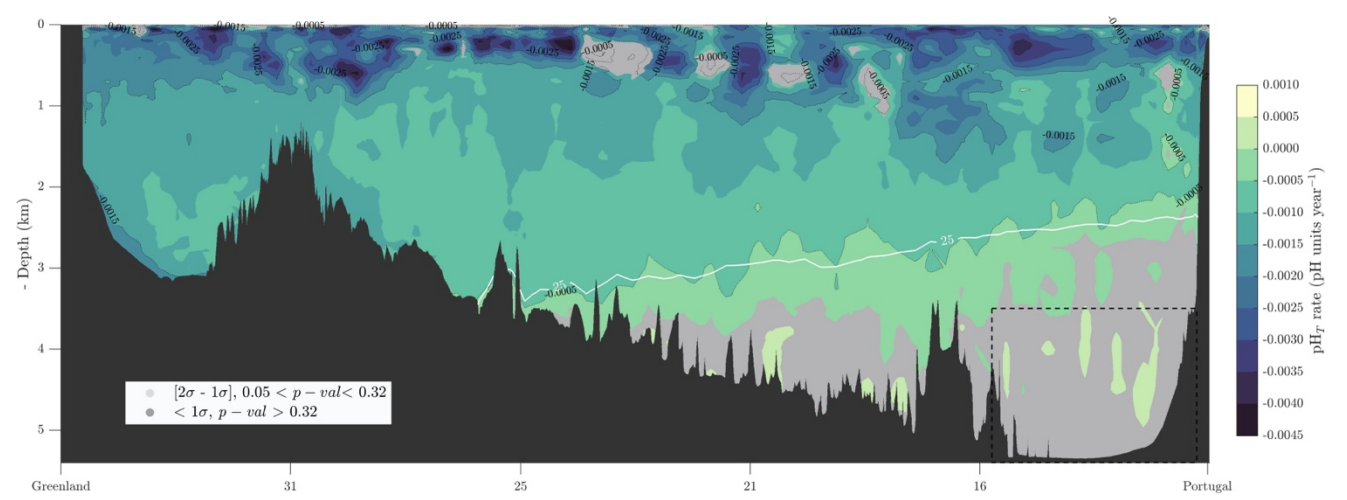


Figure 10. Linear trends in pH_T at 25°C and 1 atm from 2002 to 2023 (i.e., OA rates) along the OVIDE-BOCATS section (Fig. 1), based on high-resolution interpolations. Blue (yellow) shading indicates more (less) negative OA rates. Grey areas denote trends that are not statistically significant at the 1σ level. The white contour represents the silicate isoline of 25 μ mol kg⁻¹, and the dashed black box marks the deep Iberian Basin region used for measurement quality-control (see Sect. 4.2). Longitude (° W) is shown on the x-axis.

On the other hand, in the deep-water masses east to 30°W, there is a clear transition to non-significant OA rates at depth (Fig. 10). This transition coincides with the 25 µmol kg⁻¹ silicate isoline, which marks the boundary between NA-origin waters and those with Antarctic influence (García-Ibáñez et al., 2015). At this silicate level, García-Ibáñez et al. (2015) estimated that NEADW accounts for ~30% of the water mass composition, while LSW and ISOW contribute the remaining 70%, with proportions varying with depth. NEADW originates from Antarctic Bottom Water, formed in the Vema Fracture Zone, and is largely devoid of C_{ant} (Steinfeldt et al., 2024). Consequently, as silicate concentrations increase beyond 25 µmol kg⁻¹, the influence of NEADW becomes dominant, resulting in non-significant OA rates (Fig. 10), and elevated AOU values (Supporting Information Fig. 6a), consistent with the advanced age and limited ventilation of these waters.

5. Conclusions

We present a new, rigorously quality-controlled dataset of discrete spectrophotometric pH_T measurements from the North Atlantic, spanning over two decades and including absorbance data. This dataset provides a unique resource for the ocean carbon research community, enabling retrospective reassessment of pH_T values and derived variables under updated methodological standards.

Our analysis revealed that pH_T values measured with an unpurified mCP dye from Sigma-Aldrich exhibit a consistent positive bias of $+0.011 \pm 0.002$ pH_T units, on average, compared to those measured using purified mCP dye, with this offset decreasing slightly at higher pH_T. While the correction applied has negligible influence on previously published OA trends, it significantly affects derived variables such as the aragonite saturation horizon, which is now estimated to be up to 200 m shallower in certain regions. These changes have implications for assessing the vulnerability of deep-sea ecosystems to OA and underscore the need for highly accurate pH_T measurements.





Our results reinforce findings from recent studies (e.g., Carter et al., 2024a; Takeshita et al., 2021, 2022) and support the following recommendations:

- 1. Ideally, pH_T measurements should be carried out using well-characterized, purified mCP dyes and following consensus procedures that ensure SI traceability (Capitaine et al., 2023; Carter et al., 2024a), regardless of mCP dye used.
- 2. Although the correction applied here ($_{434}A_{imp} = 0.0034$) yielded consistent results, we recommend the determination of batch-specific $_{434}A_{imp}$ values (Douglas & Byrne, 2017; Álvarez et al., submitted).
- 3. The effect of mCP dye addition on sample pH_T is comparable in magnitude to spectrophotometer non-linearity. Our findings support the estimation of this effect via $\Delta(pH_T/_{488}A)$ -vs- $pH_{T,1}$ approach proposed by Takeshita et al. (2022), and are consistent with recommendations by Li et al. (2020).
- 4. While the mCP dye does not significantly alter the *TRIS* buffer pH_T, accurate temperature control is essential. *TRIS* remains suitable for methodological validation, with spectrophotometer behavior being the primary concern (Capitaine et al., 2023).

6. Data availability

The complete OVIDE-BOCATS pH_T dataset presented in this study is made available at https://doi.org/10.5281/zenodo.17141184 (Pérez et al., 2025) in multiple formats to ensure broad accessibility and compatibility with different research workflows. The dataset includes 23,535 spectrophotometric pH_T measurements along with associated absorbance data (434A, 578A, and 488A) and complete spatiotemporal metadata from 11 cruises spanning 2002-2023. Data are provided as: (1) comma-separated values (CSV) format for general use, (2) WHP-Exchange bottle format following WOCE Hydrographic Program Exchange format standards, (3) NetCDF format with CF-compliant metadata, and (4) Apache Parquet format with both CF standard names and the proposed metadata conventions of Jiang et al. (2022). This multi-format approach ensures the data can be readily integrated into existing oceanographic databases and analysis workflows, adhering to FAIR (Findable, Accessible, Interoperable, and Reusable) data principles. All formats include quality flags for pH_T following GLODAP recommendations.

Supplementary Information

The supplement related to this article is available online at:

Author contribution

FFP, MLM, and AV designed the study, conceptualization, methodology, validation and formal analysis. AV, PL and FFP give supervision, administration and funding. The manuscript was written by MLM and FFP and edited, and also revised by MGI and discussed by all authors. The dataset, data curation and validation were done by FFP, AV, MA and MLM.

Competing interests

Author A. Velo is a member of the editorial board of the journal.





Acknowledgments

We thank all of the scientists, technicians, personnel, and crew who were responsible for the collection and analysis of the over 23 000 samples included in the final dataset.

Financial support

F.F. Pérez and A. Padin were supported by FICARAM+ (PID2023-148924OB-I00) project funded by MICIU/AEI/10.13039/501100011033 and FEDER, UE. A. Velo was supported by the European Union under grant agreement no. 101094690 (EuroGO-SHIP). M. López-Mozos was supported by the grant PRE2020-093138 funded by MICIU/AEI/10.13039/501100011033 and by "ESF Investing in your future". M. Fontela was funded by PTA2022-021307-I, MCIN/AEI/10.13039/501100011033 and by FSE+. M.I. García-Ibáñez and M. Álvarez were supported by the ESMARES (Marine Strategy Directive Framework) program funded by the Spanish Ministry for the Ecological Transition and the Demographic Challenge. N.M. Fajar was supported the Complementary Science Plans for Marine Science of 'Ministerio de Ciencia, Innovación y Universidades' included in the Recovery, Transformation and Resilience Plan (PRTR-C17.I1) funded through 'Xunta de Galicia' with Next Generation EU and the European Maritime Fisheries and Aquaculture Fund.

This work has been supported by FICARAM+ (PID2023-148924OB-I00) project funded by MICIU/AEI /10.13039/501100011033 and FEDER, UE.

This work was co-funded by the European Union under grant agreement no. 101094690 (EuroGO-SHIP) and UK Research and Innovation (UKRI) under the UK government's Horizon Europe funding guarantee [grant numbers: 10051458, 10068242, 10068528]. Views and opinions expressed are however those of the author(s) only and do not necessarily reflect those of the European Union or European Research Executive Agency. Neither the European Union nor the granting authority can be held responsible for them.

References

Álvarez, M., Fajar, N. M., Carter, B. R., Guallart, E. F., Pérez, F. F., Woosley, R. J., & Murata, A. (2020). Global ocean spectrophotometric pH assessment: consistent inconsistencies. *Environmental Science & Technology*, 54(18), 10977-10988. https://doi.org/10.1021/acs.est.9b06932

Álvarez M., et al. "Ocean acidification at the crossroads I: harmonizing unpurified and purified meta cresol purple spectrophotometric pH measurements based on absorbance data". Limnology and oceanography: Methods, submitted.

Álvarez-Salgado, X. A., Nieto-Cid, M., Álvarez, M., Pérez, F. F., Morin, P., & Mercier, H. (2013). New insights on the mineralization of dissolved organic matter in central, intermediate, and deep water masses of the northeast North Atlantic. *Limnol. Oceanogr.*, 58(2), 681–696. https://doi.org/10.4319/lo.2013.58.2.0681

Amidror, I. (2002). Scattered data interpolation methods for electronic imaging systems: A survey. 11(2), 157–176. https://doi.org/10.1117/1.1455013

Asselot, R., Carracedo, L. I., Thierry, V., Mercier, H., Bajon, R., & Pérez, F. F. (2024). Anthropogenic carbon pathways towards the North Atlantic interior revealed by Argo-O2, neural networks and back-calculations. *Nature*





- *Communications*, *15*(1), 1630. https://doi.org/10.1038/s41467-024-46074-5
- Bushinsky, S. M., Nachod, Z., Fassbender, A. J., Tamsitt, V., Takeshita, Y., & Williams, N. (2025). Offset Between Profiling Float and Shipboard Oxygen Observations at Depth Imparts Bias on Float pH and Derived *p* CO₂. *Global Biogeochemical Cycles*, *39*(5), e2024GB008185. https://doi.org/10.1029/2024GB008185
 - Byrne, R. H., & Breland, J. A. (1989). High precision multiwavelength pH determinations in seawater using cresol red. *Deep Sea Research Part A. Oceanographic Research Papers*, *36*(5), 803–810.
 - Caldeira, K., & Wickett, M. E. (2003). Anthropogenic carbon and ocean pH. Nature, 425(6956), 365-365. https://doi.org/10.1038/425365a
 - Capitaine, G., Stoica, D., Wagener, T., & Fisicaro, P. (2023). Production of a reference material for seawater pHT measurements by a National Metrology Institute. *Marine Chemistry*, 252, 104244. https://doi.org/10.1016/j.marchem.2023.104244
 - Carter, B. R., Feely, R. A., Williams, N. L., Dickson, A. G., Fong, M. B., & Takeshita, Y. (2018). Updated methods for global locally interpolated estimation of alkalinity, pH, and nitrate. *Limnology and Oceanography: Methods*, *16*(2), 119-131. https://doi.org/10.1002/lom3.10232
 - Carter, B. R., Radich, J. A., Doyle, H. L., & Dickson, A. G. (2013). An automated system for spectrophotometric seawater pH measurements. *Limnology and Oceanography: Methods*, 11(1), 16–27. https://doi.org/10.4319/lom.2013.11.16
 - Carter, B. R., Sharp, J. D., Dickson, A. G., Alvarez, M., Fong, M. B., García-Ibáñez, M. I., ... & Wang, Z. A. (2024a). Uncertainty sources for measurable ocean carbonate chemistry variables. Limnology and Oceanography, 69(1), 1-21. https://doi.org/10.1002/lno.12477
- Carter, B. R., Sharp, J. D., García-Ibáñez, M. I., Woosley, R. J., Fong, M. B., Álvarez, M., ... & Wang, Z. A. (2024b). Random and systematic uncertainty in ship-based seawater carbonate chemistry observations. *Limnology and Oceanography*, 69(10), 2473-2488.
- 812 https://doi.org/10.1002/lno.12674
 - Chierici, M., Fransson, A., & Anderson, L. G. (1999). Influence of *m*-cresol purple indicator additions on the pH of seawater samples: Correction factors evaluated from a chemical speciation model. *Marine Chemistry*, 65(3), 281–290. https://doi.org/10.1016/S0304-4203(99)00020-1
- Clayton, T. D., & Byrne, R. H. (1993). Spectrophotometric seawater pH measurements: Total hydrogen ion concentration scale calibration of m-cresol purple and at-sea results. *Deep Sea Research Part I: Oceanographic Research Papers*, 40(10), 2115–2129. https://doi.org/10.1016/0967-0637(93)90048-8
- Daniault, N., Mercier, H., Lherminier, P., Sarafanov, A., Falina, A., Zunino, P., Pérez, F. F., Ríos, A. F., Ferron, B., Huck, T., Thierry, V., & Gladyshev, S. (2016). The northern North Atlantic Ocean mean circulation in the early 21st century. *Progress in Oceanography*, 146, 142–158. https://doi.org/10.1016/j.pocean.2016.06.007
- de la Paz, M., García-Ibáñez, M. I., Steinfeldt, R., Ríos, A. F., & Pérez, F. F. (2017). Ventilation versus biology:





836

843

847

848 849

857

865

- 827 What is the controlling mechanism of nitrous oxide distribution in the North Atlantic? Global Biogeochemical 828 Cycles, 31(4), 745–760. https://doi.org/10.1002/2016GB005507
- 829 830 DelValls, T., & Dickson, A. (1998). The pH of buffers based on 2-amino-2-hydroxymethyl-1, 3-propanediol ('tris') 831 in synthetic sea water. Deep-Sea Research Part I, 45(9), 1541-1554. https://doi.org/10.1016/s0967-832 0637(98)00019-3
- Dickson, A. G. (1993). The measurement of sea water pH. Marine chemistry, 44(2-4), 131-142. 834 835 https://doi.org/10.1016/0304-4203(93)90198-W
- 837 Dickson, A. G. (2010). Standards for ocean measurements. *Oceanography*, 23(3), 34-47. 838 https://www.jstor.org/stable/24860884 839
- 840 Dickson, A. G., Camões, M. F., Spitzer, P., Fisicaro, P., Stoica, D., Pawlowicz, R., & Feistel, R. (2015). 841 Metrological challenges for measurements of key climatological observables. Part 3: seawater pH. Metrologia, 842 53(1), R26. https://doi.org/10.1088/0026-1394/53/1/R26
- 844 Dickson, A. G., Sabine, C. L., & Christian, J. R. (2007). Guide to best practices for ocean CO₂ measurements (Vol. 845 3). http://www.oceandatapractices.org/handle/11329/249 846
 - Douglas, N. K., & Byrne, R. H. (2017). Achieving accurate spectrophotometric pH measurements using unpurified meta-cresol purple. Marine Chemistry, 190, 66-72. https://doi.org/10.1016/j.marchem.2017.02.004
- Fong, M. B., Takeshita, Y., Easley, R. A., & Waters, J. F. (2024). Detection of impurities in m-cresol purple with 850 851 Soft Independent Modeling of Class Analogy for the quality control of spectrophotometric pH measurements in 852 seawater. Marine chemistry, 259, 104362. https://doi.org/10.1038/s41598-017-02624-0 853
- 854 Fontela, M., Mercier, H., & Pérez, F. F. (2019). Long-term integrated biogeochemical budget driven by circulation 855 Atlantic. Progress Oceanography, eastern subpolar North in 51-65. 856 http://doi.org/10.1016/j.pocean.2019.02.004
- 858 Fontela, M., Pérez, F. F., Carracedo, L. I., Padín, X. A., Velo, A., García-Ibañez, M. I., & Lherminier, P. (2020a). 859 The Northeast Atlantic is running out of excess carbonate in the horizon of cold-water corals communities. 860 Scientific Reports, 10(1), Article 1. https://doi.org/10.1038/s41598-020-71793-2 861
- 862 Fontela, M., Pérez, F. F., Mercier, H., & Lherminier, P. (2020b). North Atlantic western boundary currents are 863 dissolved intense organic carbon streams. Frontiers in Marine Science, 7, 593757. 864 https://doi.org/10.3389/fmars.2020.593757
- 866 Fontela, M., Velo, A., Brown, P.J., Pérez, F.F. (2023). Carbonate System Species and pH. In: Blasco, J., Tovar-867 Sánchez, A. (eds) Marine Analytical Chemistry. Springer, Cham. https://doi.org/10.1007/978-3-031-14486-8 1
- 869 Friedlingstein, P., O'Sullivan, M., Jones, M. W., Andrew, R. M., Bakker, D. C. E., Hauck, J., Landschützer, P., Le 870 Quéré, C., Luijkx, I. T., Peters, G. P., Peters, W., Pongratz, J., Schwingshackl, C., Sitch, S., Canadell, J. G., Ciais,
- 871 P., Jackson, R. B., Alin, S. R., Anthoni, P., ... Zheng, B. (2023). Global Carbon Budget 2023. Earth System Science
- 872 Data, 15(12), 5301–5369. https://doi.org/10.5194/essd-15-5301-2023



877

881

885

891 892

893

894

895

896 897

898

899

900 901

902

903

904

905



- García-Ibáñez, M. I., Bates, N. R., Bakker, D. C. E., Fontela, M., & Velo, A. (2021). Cold-water corals in the Subpolar North Atlantic Ocean exposed to aragonite undersaturation if the 2 °C global warming target is not met. *Global and Planetary Change*, 201, 103480. https://doi.org/10.1016/j.gloplacha.2021.103480
- García-Ibáñez, M. I., Pardo, P. C., Carracedo, L. I., Mercier, H., Lherminier, P., Ríos, A. F., & Pérez, F. F. (2015). Structure, transports and transformations of the water masses in the Atlantic Subpolar Gyre. *Progress in Oceanography*, *135*, 18–36. https://doi.org/10.1016/j.pocean.2015.03.009
- García-Ibáñez, M. I., Zunino, P., Fröb, F., Carracedo, L. I., Ríos, A. F., Mercier, H., Olsen, A., & Pérez, F. F. (2016). Ocean acidification in the subpolar North Atlantic: Rates and mechanisms controlling pH changes. *Biogeosciences*, 13(12), 3701–3715. https://doi.org/10.5194/bg-13-3701-2016
- 886 Gattuso, J.-P., Magnan, A., Billé, R., Cheung, W. W. L., Howes, E. L., Joos, F., Allemand, D., Bopp, L., Cooley, 887 S. R., Eakin, C. M., Hoegh-Guldberg, O., Kelly, R. P., Pörtner, H.-O., Rogers, A. D., Baxter, J. M., Laffoley, D., 888 Osborn, D., Rankovic, A., Rochette, J., ... Turley, C. (2015). Contrasting futures for ocean and society from anthropogenic 889 different CO_2 emissions scenarios. Science, 349(6243), aac4722. 890 https://doi.org/10.1126/science.aac4722
 - Gehlen, M., Séférian, R., Jones, D. O. B., Roy, T., Roth, R., Barry, J., Bopp, L., Doney, S. C., Dunne, J. P., Heinze, C., Joos, F., Orr, J. C., Resplandy, L., Segschneider, J., & Tjiputra, J. (2014). Projected pH reductions by 2100 might put deep North Atlantic biodiversity at risk. *Biogeosciences*, 11(23), 6955–6967. https://doi.org/10.5194/bg-11-6955-2014
 - IPCC. (2019). IPCC Special Report on the Ocean and Cryosphere in a Changing Climate [H.- O. Pörtner, D.C. Roberts, V. Masson-Delmotte, P. Zhai, M. Tignor, E. Poloczanska, K. Mintenbeck, M. Nicolai, A. Okem, J. Petzold, B. Rama, N. Weyer (eds.)]. Intergovernmental Panel on Climate Change.
 - Ishii, M., Carter, B. R., Toyama, K., Rodgers, K. B., Feely, R. A., Chau, T.-T.-T., Chevallier, F., Desmet, F., Gregor, L., Iida, Y., Kitamura, Y., Müller, J. D., & Tsujino, H. (2025). CO2 Uptake in the Pacific From 1985 to 2018: A Comparative Assessment of Observation- and Model-Based Estimates. *Global Biogeochemical Cycles*, 39(5), e2024GB008355. https://doi.org/10.1029/2024GB008355
- Jiang, L.Q., Pierrot, D., Wanninkhof, R., Feely, R.A., Tilbrook, B., Alin, S., Barbero, L., Byrne, R.H., Carter, B.R.,
 Dickson, A.G., Gattuso, J.P., Greeley, D., Hoppema, M., Humphreys, M.P., Karstensen, J., Lange, N., Lauvset,
 S.K., Lewis, E.R., Olsen, A., Pérez, F.F., Sabine, C., Sharp, J.D., Tanhua, T., Trull, T.W., Velo, A., Allegra, A.J.,
 Barker, P., Burger, E., Cai, W.J., Chen, C.T.A., Cross, J., Garcia, H., Hernandez-Ayon, J.M., Hu, X., Kozyr, A.,
 Langdon, C., Lee, K., Salisbury, J., Wang, Z.A., Xue, L., 2022. Best Practice Data Standards for Discrete Chemical
 Oceanographic Observations. Front. Mar. Sci. 8, 2099. https://doi.org/10.3389/fmars.2021.705638
- Key, R.M., Olsen, A., van Heuven, S., Lauvset, S.K., Velo, A., Lin, X., Schirnick, C., Kozyr, A., Tanhua, T., Hoppema, M., Jutterstrom, S., Steinfeldt, R., Jeansson, E., Ishi, M., Perez, F.F., & Suzuki, T. (2015). *Global Ocean*
- 915 Data Analysis Project, Version 2 (GLODAPv2), ORNL/CDIAC-162, ND-P093. Carbon Dioxide Information
- 916 Analysis Center (CDIAC). http://dx.doi.org/10.3334/CDIAC/OTG.NDP093_GLODAPv2
 917
- Wiatkowski, L., & Orr, J. C. (2018). Diverging seasonal extremes for ocean acidification during the twenty-first





- 919 century. *Nature Climate Change*, 8(2), 141–145. https://doi.org/10.1038/s41558-017-0054-0
- Lauvset, S. K., Lange, N., Tanhua, T., Bittig, H. C., Olsen, A., Kozyr, A., ... & Key, R. M. (2024). The annual update GLODAPv2. 2023: the global interior ocean biogeochemical data product. Earth System Science Data, 16(4), 2047-2072. https://doi.org/10.5194/essd-16-2047-2024
- Le Quéré, C., Moriarty, R., Andrew, R. M., Canadell, J. G., Sitch, S., Korsbakken, J. I., Friedlingstein, P., Peters,
 G. P., Andres, R. J., Boden, T. A., Houghton, R. A., House, J. I., Keeling, R. F., Tans, P., Arneth, A., Bakker, D.
 C. E., Barbero, L., Bopp, L., Chang, J., ... Zeng, N. (2015). Global Carbon Budget 2015. *Earth System Science Data*, 7(2), 349–396. https://doi.org/10.5194/essd-7-349-2015
- Lee, K., Kim, T. W., Byrne, R. H., Millero, F. J., Feely, R. A., & Liu, Y. M. (2010). The universal ratio of boron to chlorinity for the North Pacific and North Atlantic oceans. *Geochimica et Cosmochimica Acta*, 74(6), 1801-1811. https://doi.org/10.1016/j.gca.2009.12.027
 - Lee, K., Millero, F. J., Byrne, R. H., Feely, R. A., & Wanninkhof, R. (2000). The recommended dissociation constants for carbonic acid in seawater. *Geophysical Research Letters*, 27(2), 229–232. https://doi.org/10.1029/1999GL002345
 - Lherminier, P., Mercier, H., Huck, T., Gourcuff, C., Perez, F. F., Morin, P., Sarafanov, A., & Falina, A. (2010). The Atlantic Meridional Overturning Circulation and the subpolar gyre observed at the A25-OVIDE section in June 2002 and 2004. *Deep Sea Research Part I: Oceanographic Research Papers*, 57(11), 1374–1391. https://doi.org/10.1016/j.dsr.2010.07.009
 - Li, X., García-Ibáñez, M. I., Carter, B. R., Chen, B., Li, Q., Easley, R. A., & Cai, W.-J. (2020). Purified meta-Cresol Purple dye perturbation: How it influences spectrophotometric pH measurements. *Marine Chemistry*, 225, 103849. https://doi.org/10.1016/j.marchem.2020.103849
 - Liu, X., Patsavas, M. C., & Byrne, R. H. (2011). Purification and Characterization of meta-Cresol Purple for Spectrophotometric Seawater pH Measurements. *Environmental Science & Technology*, 45(11), 4862–4868. https://doi.org/10.1021/es200665d
- Loucaides, S., Rèrolle, V. M., Papadimitriou, S., Kennedy, H., Mowlem, M. C., Dickson, A. G., ... & Achterberg, E. P. (2017). Characterization of meta-Cresol Purple for spectrophotometric pH measurements in saline and hypersaline media at sub-zero temperatures. *Scientific reports*, 7(1), 2481. https://doi.org/10.1038/s41598-017-02624-0
 - Lueker, T. J., Dickson, A. G., & Keeling, C. D. (2000). Ocean pCO2 calculated from dissolved inorganic carbon, alkalinity, and equations for K1 and K2: Validation based on laboratory measurements of CO2 in gas and seawater at equilibrium. *Marine Chemistry*, 70(1–3), 105–119. https://doi.org/10.1016/S0304-4203(00)00022-0
- Ma, J., Shu, H., Yang, B., Byrne, R. H., & Yuan, D. (2019). Spectrophotometric determination of pH and carbonate ion concentrations in seawater: Choices, constraints and consequences. *Analytica Chimica Acta*, 1081, 18-31. https://doi.org/10.1016/j.aca.2019.06.024
- Maurer, T. L., Plant, J. N., & Johnson, K. S. (2021). Delayed-Mode Quality Control of Oxygen, Nitrate, and pH



976

987

988

989

990

991 992

993

994

995 996

997

998

999

1003



- 965 Data **SOCCOM** Biogeochemical **Profiling** Floats. **Frontiers** Marine Science, 8. 966 https://doi.org/10.3389/fmars.2021.683207 967
- 968 Mercier, H., Desbruyères, D., Lherminier, P., Velo, A., Carracedo, L., Fontela, M., & Pérez, F. F. (2024). New 969 insights into the eastern subpolar North Atlantic meridional overturning circulation from OVIDE. Ocean Science, 970 20(3), 779–797. https://doi.org/10.5194/os-20-779-2024
- 972 Müller, J. D., Bastkowski, F., Sander, B., Seitz, S., Turner, D. R., Dickson, A. G., & Rehder, G. (2018). Metrology 973 for pH measurements in Brackish Waters—part 1: Extending electrochemical pH T measurements of TRIS buffers 974 to salinities 5-20. Frontiers in Marine Science, 5, 176. 975
 - https://doi.org/10.3389/fmars.2018.00176
- 977 Olsen, A., Key, R. M., van Heuven, S., Lauvset, S. K., Velo, A., Lin, X., Schirnick, C., Kozyr, A., Tanhua, T., 978 Hoppema, M., Jutterström, S., Steinfeldt, R., Jeansson, E., Ishii, M., Pérez, F. F., & Suzuki, T. (2016). The Global 979 Ocean Data Analysis Project version 2 (GLODAPv2) – an internally consistent data product for the world ocean. Earth System Science Data, 8(2), 297–323. https://doi.org/10.5194/essd-8-297-2016 980 981
- 982 Olsen, A., Lange, N., Key, R. M., Tanhua, T., Álvarez, M., Becker, S., Bittig, H. C., Carter, B. R., Cotrim da 983 Cunha, L., Feely, R. A., van Heuven, S., Hoppema, M., Ishii, M., Jeansson, E., Jones, S. D., Jutterström, S., Karlsen, 984 M. K., Kozyr, A., Lauvset, S. K., ... Wanninkhof, R. (2019). GLODAPv2.2019 – an update of GLODAPv2. Earth 985 System Science Data, 11(3), 1437–1461. https://doi.org/10.5194/essd-11-1437-2019 986
 - Orr, J. C., Fabry, V. J., Aumont, O., Bopp, L., Doney, S. C., Feely, R. A., Gnanadesikan, A., Gruber, N., Ishida, A., Joos, F., Key, R. M., Lindsay, K., Maier-Reimer, E., Matear, R., Monfray, P., Mouchet, A., Najjar, R. G., Plattner, G.-K., Rodgers, K. B., ... Yool, A. (2005). Anthropogenic ocean acidification over the twenty-first century and its impact on calcifying organisms. Nature, 437, 681–686. https://doi.org/10.1038/nature04095
 - Pérez, F. F., Fontela, M., García-Ibáñez, M. I., Mercier, H., Velo, A., Lherminier, P., Zunino, P., Paz, M. de la, Alonso-Pérez, F., Guallart, E. F., & Padin, X. A. (2018). Meridional overturning circulation conveys fast acidification to the deep Atlantic Ocean. Nature, 554(7693), 515–518. https://doi.org/10.1038/nature25493
 - Pérez, F. F., López-Mozos, M., Fontela, M., García-Ibáñez, M. I., Fajar, N. M., Padin, X. A., Castaño-Carrera, M., de la Paz, M., Carracedo, L. I., Ávarez, M., Lherminier, P., & Velo, A. (2025). Two decades of pHT measurements along the GO-SHIP A25 section - Dataset [Data set]. Zenodo. https://doi.org/10.5281/zenodo.17141184
- 1000 Pérez, F. F., Mercier, H., Vázquez-Rodríguez, M., Lherminier, P., Velo, A., Pardo, P. C., Rosón, G., & Ríos, A. F. 1001 (2013). Atlantic Ocean CO₂ uptake reduced by weakening of the meridional overturning circulation. Nature 1002 Geoscience, 6(2), 146–152. https://doi.org/10.1038/ngeo1680
- 1004 Pérez, F. F., Olafsson, J., Ólafsdóttir, S. R., Fontela, M., & Takahashi, T. (2021). Contrasting drivers and trends of 1005 ocean acidification in the subarctic Atlantic. Scientific Reports, 11(1), Article 1. https://doi.org/10.1038/s41598-1006 021-93324-3
- 1008 Pérez, F. F., Perez, F. F., Becker, M., Goris, N., Gehlen, M., Lopez-Mozos, M., Tjiputra, J., Olsen, A., Müller, J. 1009 D., Huertas, I. E., Chau, T. T., Cainzos, V., Velo, A., Benard, G., Hauck, J., Gruber, N., & Wanninkhof, R.
- 1010 (2023). An assessment of CO2 storage and sea-air fluxes for the Atlantic Ocean and Mediterranean Sea between





- 1011 1985 and 2018 [Preprint]. Preprints. https://doi.org/10.22541/essoar.170256825.55098483/v2
- Ramette, R. W., Culberson, C. H., & Bates, R. G. (1977). Acid-base properties of tris(hydroxymethyl)aminomethane (Tris) buffers in sea water from 5 to 40.degree.C. *Analytical Chemistry*, 49(6), 867–870. https://doi.org/10.1021/ac50014a049
- Resplandy, L., Bopp, L., Orr, J. C., & Dunne, J. P. (2013). Role of mode and intermediate waters in future ocean acidification: Analysis of CMIP5 models. *Geophysical Research Letters*, 40(12), 3091–3095. https://doi.org/10.1002/grl.50414
 - Rivaro, P., Vivado, D., Falco, P., & Ianni, C. (2021). HPLC-DAD Purification and Characterization of Meta-Cresol-Purple for Spectrophotometric Seawater pH Measurements. *Water*, *13*(21), Article 21. https://doi.org/10.3390/w13213030
 - Rodgers, K. B., Schwinger, J., Fassbender, A. J., Landschützer, P., Yamaguchi, R., Frenzel, H., Stein, K., Müller, J. D., Goris, N., Sharma, S., Bushinsky, S., Chau, T.-T.-T., Gehlen, M., Gallego, M. A., Gloege, L., Gregor, L., Gruber, N., Hauck, J., Iida, Y., ... Velo, A. (2023). Seasonal Variability of the Surface Ocean Carbon Cycle: A Synthesis. *Global Biogeochemical Cycles*, *37*(9), e2023GB007798. https://doi.org/10.1029/2023GB007798
 - Sabine, C. L., Feely, R. A., Gruber, N., Key, R. M., Lee, K., Bullister, J. L., Wanninkhof, R., Wong, C. S., Wallace, D. W. R., Tilbrook, B., Millero, F. J., Peng, T.-H., Kozyr, A., Ono, T., & Rios, A. F. (2004). The Oceanic Sink for Anthropogenic CO₂. *Science*, 305(5682), 367–371. https://doi.org/10.1126/science.1097403
 - Steinfeldt, R., Rhein, M., & Kieke, D. (2024). Anthropogenic carbon storage and its decadal changes in the Atlantic between 1990–2020. *Biogeosciences*, 21(16), 3839–3867. https://doi.org/10.5194/bg-21-3839-2024
 - Takeshita, Y., Johnson, K. S., Coletti, L. J., Jannasch, H. W., Walz, P. M., & Warren, J. K. (2020). Assessment of pH dependent errors in spectrophotometric pH measurements of seawater. *Marine Chemistry*, 223, 103801. https://doi.org/10.1016/j.marchem.2020.103801
 - Takeshita, Y., Johnson, K. S., Martz, T. R., Plant, J. N., & Sarmiento, J. L. (2018). Assessment of Autonomous pH Measurements for Determining Surface Seawater Partial Pressure of CO2. *Journal of Geophysical Research: Oceans*, 123(6), 4003–4013. https://doi.org/10.1029/2017JC013387
 - Takeshita, Y., Mertz, K. L., Norgaard, A., Gray, S., Verburg, M. H., & Bockmon, E. E. (2022). Accurate spectrophotometric pH measurements made directly in the sample bottle using an aggregated dye perturbation approach. *Limnology and Oceanography: Methods*, 20(5), 281–287. https://doi.org/10.1002/lom3.10486
- Takeshita, Y., Warren, J. K., Liu, X., Spaulding, R. S., Byrne, R. H., Carter, B. R., DeGrandpre, M. D., Murata, A., & Watanabe, S. (2021). Consistency and stability of purified meta-cresol purple for spectrophotometric pH measurements in seawater. *Marine Chemistry*, 236, 104018. https://doi.org/10.1016/j.marchem.2021.104018
- Vázquez-Rodríguez, M., Pérez, F. F., Velo, A., Ríos, A. F., & Mercier, H. (2012). Observed acidification trends in North Atlantic water masses. *Biogeosciences*, *9*(12), 5217–5230. https://doi.org/10.5194/bg-9-5217-2012
- Woosley, R. J. 2021. Long-term stability and storage of meta-cresol purple solutions for seawater pH measurements. Limnol Oceanogr Methods 19: 810–817. doi:10.1002/LOM3.10462.

https://doi.org/10.5194/essd-2025-476 Preprint. Discussion started: 20 October 2025 © Author(s) 2025. CC BY 4.0 License.





Yao, W., Liu, X., & Byrne, R. H. (2007). Impurities in indicators used for spectrophotometric seawater pH measurements: Assessment and remedies. *Marine Chemistry*, 107(2), 167–172.

Zunino, P., Lherminier, P., Mercier, H., Padín, X. A., Ríos, A. F., & Pérez, F. F. (2015). Dissolved inorganic carbon budgets in the eastern subpolar North Atlantic in the 2000s from in situ data. *Geophysical Research Letters*, 42(22), 9853-9861. https://doi.org/10.1002/2015GL066243